# Chapter I

# Introduction

> الحب ومَا يولده.
> وَالتمرد ومَا يوجده.
> وَالحرية ومَا تنميه.
> ثلَاثة مظَاهر من مظَاهر اللّٰه.
> Love and what generates it.
> Rebellion and what creates it.
> Liberty and what nourishes it.
> Three manifestations of God.
>
> *The Vision* by Kahlil Gibran,
> translation by Juan R. I. Cole

## I.1 The Birth of a Bubble

Like our own, the life of each bubble begins with *love*, in this case, the love of its *mother phase*. Unlike other liquids, a mother phase has an abundance of dissolved gas that it selflessly gives away to nourish the birth and growth of bubbles. This condition is called supersaturation—in the case of a bottle of pop[1], the liquid becomes a supersaturated mother phase upon releasing the pressure by opening the cap. Through thermal fluctuations in the density of dissolved gas, some molecules of will cluster and separate from the liquid to form the beginning of a new bubble. Just as a mother does not easily give away her child, neither does the liquid mother phase easily permit this cluster of gas molecules to separate into its own bubble. For a bubble to be born, it must *rebel*. We call this rebellion *nucleation*. Tension arises from this conflict, which resists the separation of the new bubble. All along the surface of the cluster of gas molecules, the liquid molecules of the mother phase are pulling on each other, resulting in a force that resists the rebellion of the bubble aptly named "interfacial tension." This tension not only resists the growth of the bubble but seeks to dissolve it back into the loving embrace of the mother phase. The gas tries in vain to break free from its mother phase on its own, but is often

---

[1] Regional variation on the more common but less fun "soda."

overwhelmed by the cost of independence and dissolves back into the liquid. Those whose rebellions are successful arrive at the third stage: *liberty*. The gas has now become its own bubble and continues to grow in its new life. From this starting point, a bubble may grow to provide life for marine animals, fizz in a can of pop, or one of the many voids in the foam padding you might be sitting on right now. In the case of a bottle of pop, bubbles grow until they ultimately rise and form a foam at the top of the beverage. Note, however, that this growth, while only reached through rebellion, is entirely fueled by the diffusion of dissolved gas that the mother phase lovingly provides.

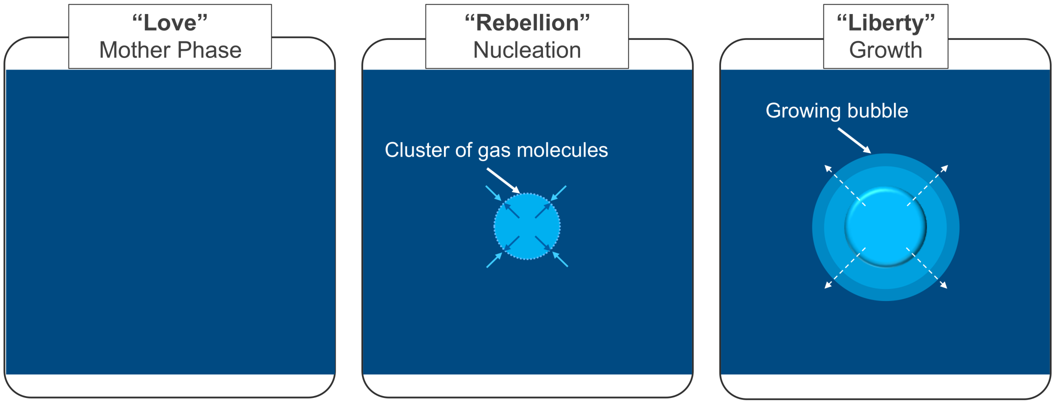

Figure I.1: Schematic of the three stages of a bubble's life. First, the love of the supersaturated mother phase provides fertile ground for the birth of a bubble. Density fluctuations of the dissolved gas lead to temporary clusters of gas that are resisted by the interfacial tension along the interface with the mother phase. If the bubble can overcome the resistance of the mother phase, it reaches the liberty of growth thereafter. Note that, while a bubble must rebel to grow up, its growth is fueled by the abundance of dissolved gas provided by the mother phase.

## I.2 The Many Causes of Bubble Nucleation

Bubbles nucleate through a variety of pathways. In each case, the liquid-like mother phase must become supersaturated, meaning that thermodynamics prefers the formation of a vapor-like bubble. The mother phase can always be supersaturated by two changes to state variables of the system: (1) increasing temperature and (2) decreasing pressure. Examples include (1) superheating water and (2) cavitation. In the case of a multicomponent system with dissolved gas, supersaturation can also be reached by increasing the concentration of dissolved gases, such as when mixing baking soda and vinegar produces carbon dioxide bubbles that provide its famous "volcano eruption."

A supersaturated mother phase can produce a bubble in four ways, which have been carefully described in the review by Jones *et al.* [1]. The most similar to the process depicted in Figure I.1 is *homogeneous nucleation*. In this process, thermal fluctuations in the local density of dissolved gas yield a cluster of molecules large enough to overcome the resistance of interfacial tension and continue to grow. This nucleation can occur throughout the mother phase without the assistance of any other component, leading to its name "homogeneous nucleation." A similar process called *heterogeneous nucleation* may occur along a surface, which may reduce the resistance faced by interfacial tension and, therefore, decrease the size of the cluster of gas molecules needed to continue to grow into a bubble.

Most bubbles would agree, however, that assembling a large enough cluster of gas molecules to overcome interfacial tension is a difficult and unlikely process. Its difficulty is why almost every bubble we have ever seen has avoided it entirely. Instead, bubbles we see in daily life generally form from the growth of entrained gas bubbles, such as when pouring a glass of pop, or gas trapped in crevices along rough surfaces, such as along the groove found at the bottom of many champagne flutes [2]. Even bubbles in boiling water come from trapped gas. Such an entrained gas bubble is called a "Harvey nucleus" [3]). Harvey *et al.* reasoned that these pockets of vapor can persist well below saturation because the solvophobicity (hydrophobicity in the case of water) of the surface causes a high enough curvature of the vapor–liquid interface for the interfacial tension to maintain enough pressure to prevent the gas from escaping. Therefore, such pockets of gas are difficult to remove, and due to the ease with which they can grow into bubbles, deplete the available dissolved gas well before true homogeneous or heterogeneous nucleation in the absence of existing bubbles become frequent enough to be observed.

Because nucleation of bubbles from these pockets of gas occurs readily and regularly at specific nucleation sites, it is easy to locate and, therefore, has been measured with greater precision. For example, in Figure I.2, compare the observation of (a) nucleation from a crevice and (b) homogeneous nucleation. While most nucleation from surfaces occurs from trapped pockets of gas rather than the chance clustering of molecules of dissolved gas, we will use the term "heterogeneous bubble nucleation" to refer to both since both occur along surfaces rather than in the bulk of the mother phase.

When homogeneous bubble nucleation does occur, it is more widespread and rapid than heterogeneous bubble nucleation because bubbles can nucleate from any

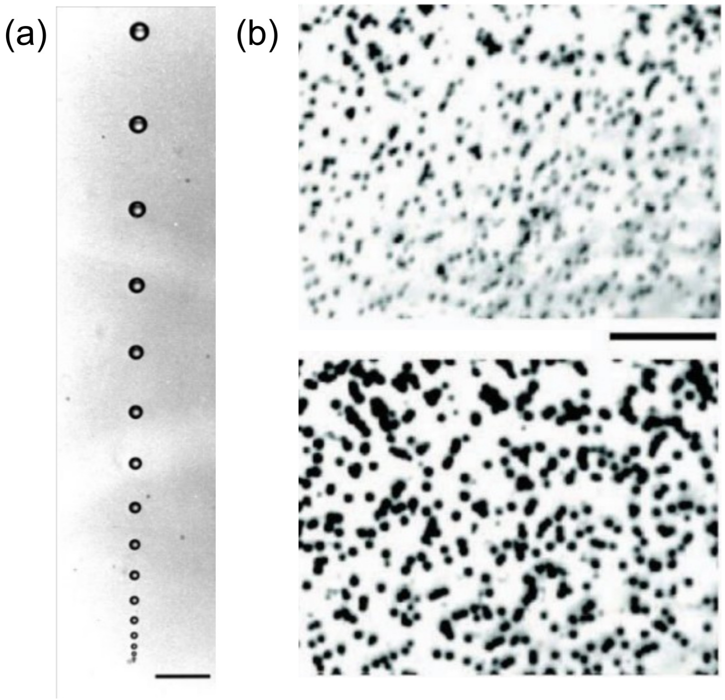

Figure I.2: (a) Observation of nucleation of carbon dioxide bubbles from a pocket of gas trapped in a crevice along the wall of a glass of a champagne (scale bar is 1 mm). Reprinted (adapted) with permission from Gérard Liger-Belair. "The physics and chemistry behind the bubbling properties of champagne and sparkling wines: A state-of-the-art review". In: *Journal of Agricultural and Food Chemistry* 53.8 (2005), pp. 2788–2802. issn: 00218561. doi: 10.1021/jf048259e. Copyright 2005 American Chemical Society. (b) Observation of homogeneous nucleation of carbon dioxide bubbles during the foaming of polystyrene (scale bar 400 $\mu$m). Note the regular nucleation of the champagne bubbles from a single nucleation site in comparison to the random nucleation of the bubbles in the polystyrene foam. Reused with permission from John Wiley and Sons [4].

point in the liquid bulk. This process can be catastrophic in the case of contact vapor explosions, in which a liquid is so superheated (often to about 90% of its critical temperature) that it boils homogeneously, creating an explosion of vapor that poses hazards in metallurgy, handling of liquefied natural gas, and nuclear reactors [5]. Nucleating bubbles from pockets of gas may be easier, but shortcuts limit potential. In the context of the present work, however, rapid and widespread bubble nucleation like this can be a boon to producing fine-celled polymer foams, so homogeneous nucleation will be our focus.

## I.3 Foams: When Many Bubbles Collide

When enough bubbles nucleate in close proximity, they can form a "foam," a liquid or solid matrix with gas dispersed inside [6]. The pores containing the gas are called "cells," which may form a continuous network (open-cell foam) or may be separated from each other by thin solid films (closed-cell foam). Foams are commonly used as lighter replacements for solid materials, both by humans (structural foams) and nature (bones, wood, etc.). Often, less is more, and foams achieve superior properties over their fully solid counterparts. For example, flexible polyurethane foams provide cushioning to sitters, sleepers, and drivers around the world [7] that solid materials could not. Drinkers may enjoy a foamy head atop their beer [8] or a foamy *collerette* ring about their glasses of champagne [2]. Foam padding in helmets has saved many lives, foam earplugs have protected the hearing of many ears, and foam sugar (marshmallows) has completed many s'mores. Not all foams are beneficial, however. Foams that form over wastewater treatment reservoirs restrict oxygen flow and reduce the amount of biomass needed to clean the water [9]. Whether good or bad, foams and how they form are important for us to understand.

While some foams are produced simply by entraining gas inside the liquid or solid matrix, as in foaming soap dispensers and when whipping egg whites for a foamy meringue, many are produced by nucleating clusters of bubbles by the mechanisms discussed in Section I.2. In all cases, a foam needs to begin with a low enough viscosity to allow cells to form, whether by entrainment of gas or expansion of bubbles. Once the cells have formed, the foam may collapse due to drainage of the liquid and coalescence of the cells if the viscosity is not reduced, as in the case of soapy foams. For this reason, foams are typically cured or vitrified to solidify the cells in place. In a meringue, air is entrained into runny egg whites while the foam is fixed in place by baking. In polymer foams, two methods are used to solidify the polymer. First, in thermoplastic foams, such as polystyrene once used to make insulating cups for hot beverages, the polymer is cooled down below its glass transition temperature $T_g$ ($\approx$ 100–107 °C for $M_w > 20$ kg/mol [10]) after foaming, causing vitrification of the polymer matrix. Second, in thermoset foams, such as polyurethane used in cushioning, acoustic insulation, and thermal insulation, a chemical reaction crosslinks the polymer reactants.

While the structure of a foam is affected by bubble growth and coarsening, as well as changes in the liquid mother phase like cross-linking or vitrification, bubble nucleation sets much of the structure of polymer foams before these changes take place. Indeed, the final bubble size distribution is more sensitive to the parameters governing bubble nucleation than those governing bubble growth [11]. The production of a desired foam—or the prevention of an undesirable foam—therefore relies on control of bubble nucleation.

### Nucleating More Bubbles for Better Polyurethane Thermal Insulation

Among these types of foams, rigid polyurethane foam (RPUF), a closed-cell thermoset foam used for thermal insulation, poses a unique opportunity for practical application and scientific inquiry. RPUFs are the leading, low-cost thermal insulation material, exceeded only by relatively high-cost aerogels [12]. RPUF's exceptionally low thermal conductivity ($\approx$ 20 mW/(m.K) [12]—see comparison in Figure **??**), ability to cure in place, 30x expansion to form tight seals, and low cost have made it the insulation of choice for refrigeration units, coolers, and even the fuel tanks for the space shuttles [13] (although RPUF was implicated in the tragic explosion of the *Columbia* space shuttle in 2003 [14]). Unfortunately, its low thermal conductivity initially relied on the low thermal conductivity of high-molecular weight volatile compounds like chlorofluorocarbons (CFCs). As discussed in the following section on $CO_2$-blown foams, these compounds and some of their successors deplete the ozone and contribute to global warming, so regulations have gradually phased them out of production.

Despite the history of environmental hazard caused by RPUFs, they play an essential role in energy conservation by providing a low-cost, easy manufacture, and extremely low thermal conductivity thermal insulation. Retrofitting a building with high-performance thermal insulation like RPUFs can often be the most effective way to reduce the energy consumption of buildings. In some cases, it may even be more economical than investing in solar and wind energy [15]. Given that over 10% of global energy consumption is used to control the temperature of buildings [15], it should not be surprising that RPUFs accounted for $\approx$2% of global plastic production in 2010 [16].

While the seriousness of ozone depletion and global warming demands more environmentally friendly formulations for the production of RPUFs, the importance of high-quality thermal insulation to everyday living motivates investigation into alternative methods of reducing the thermal conductivity of RPUFs. Reducing the thermal conductivity of an insulating foam can focus on any of three major forms of heat transfer: conduction through the solid, conduction through the gas, and radiation [17] (convection is negligible for foams with cells smaller than 4 mm) [18].

The contribution to the thermal conductivity by the solid is proportional to the solid volume fraction times the thermal conductivity of the solid (refer to equation 2 of [19]). Therefore, reducing conduction through the solid can be achieved by changing the chemistry of the solid matrix to have a lower inherent thermal conductivity or reducing the volume fraction of the solid. Each is difficult to improve upon in RPUFs: changing the chemistry can negatively impact other desirable properties like fast cure time and rigidity and further reduction in the solid fraction of the foam below its current value around 3% [16] may compromise its structural integrity.

The contribution to the thermal conductivity by conduction through the gas is generally proportional to the thermal conductivity of the gas. The thermal conductivity of a simple gas is inversely proportional to the square-root of its molecular weight according to the Chapman–Enskog formula. Therefore, RPUF manufacturers preferred to use the larger CFC molecules over the small $CO_2$ molecule to keep gas conductivity low (see reduction in gas conductivity in RPUF blown with HCFC–$H_2O$ vs. other blowing agents in Fig. **??**). With increasing regulation of such chemical (see discussion in following subsection on $CO_2$-blown foams) and flammability concerns with currently used hydrocarbons like cyclopentane, the options for high-molecular-weight blowing agents are decreasing.

Instead, further reduction in gas conductivity may require structural rather than chemical changes to the foam. If the pore size in a foam is on the order of the mean free path of the gas, the effective mean free path of the gas will be reduced. Known as the "Knudsen effect," this reduction in the mean free path reduces the thermal conductivity of the gas. The Knudsen effect has been demonstrated in nanocellular polymer foams [21] (further discussion in following Section on $CO_2$-blown foams), but nanocellular foams have not become commercially viable yet due to high costs of processing at the high pressures (> 30 MPa [22]) required.

Surprisingly, one of the more viable targets for reducing the thermal conductivity of RPUFs is the radiative heat transfer, *i.e.* the transmission of infrared radiation (IR) through the foam. Thermally insulating foams are produced with low solid fraction (3 % solid or less for polyurethane foams [16]) to minimize weight, material cost, and heat conduction through the solid component. Foams with such a low solid fraction permit a significant amount of radiative heat transfer (up to

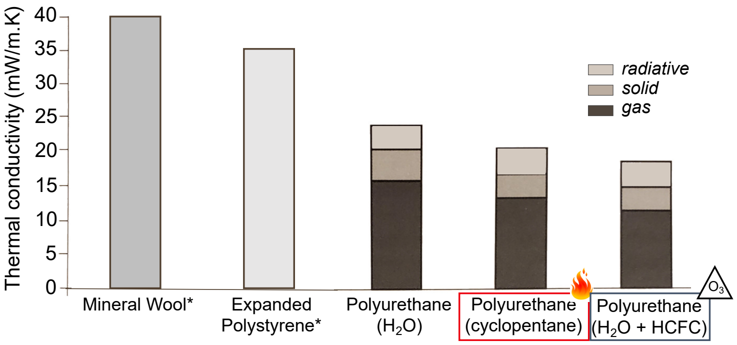

Figure I.3: Comparison of the thermal conductivity at 10 °C of different thermal insulation. The right three foams are polyurethane blown with the blowing agent(s) listed; the flammability hazard of cyclopentane and ozone-depletion hazard of HCFCs (hydrochlorofluorocarbons) is noted. The thermal conductivities of the polyurethane foams are broken down into contributions by heat transfer through radiation (top), solid conduction (middle), and gas conduction (bottom). Estimates of thermal conductivity of mineral wool and expanded polystyrene from Simpson et al. [20]. Figure adapted from Figure 15-5 of *The Polyurethanes Book* edited by David Randall and Steve Lee (2002). Made available by the US EPA Health & Environmental Research Online (HERO) database, HERO ID 4159100.

25 % of the overall heat transfer [17]) because IR radiation is easily transmitted through the gas in the cells and the thin films of polymer that separate them. In polyurethane foams, the struts at the junctions between these thin films (an example is circled in the SEM micrograph in the middle of Figure I.4) constitute 80–90 % of the solid mass [19] and are thick enough to absorb IR radiation and re-radiate it in different directions, which slows radiative heat transfer. Therefore, struts are the key to reducing radiative heat transfer through low-density foams.

Given a foam with a fixed fraction of solid material, the thermal conductivity through radiation can be most reliably decreased by decreasing the cell size, as shown in Figure I.5a. With a fixed solid fraction, decreasing cell size requires a commensurate increase in the number of cells. While the volume of solid in the struts remains the same as the cell size decreases and cell number increases, the surface area of the struts increases, increasing the likelihood that an infrared photon is absorbed and randomly re-radiated. A schematic of this effect is shown in a 2D lattice in Figure I.5b,c. As a result, the rate of radiative heat transfer is lower as the number of cells increases and their size decreases. Moreno derived a quantitative model consistent with this qualitative picture of radiative heat transfer through a foam. Moreno found that for a foam with a fixed solid volume fraction and fixed fraction of solid in the struts, the extinction coefficient is inversely proportional to

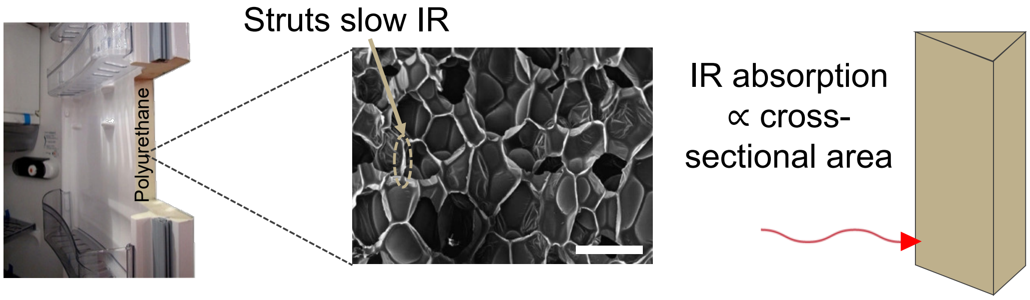

Figure I.4: Left: inside of a refrigerator door reveals polyurethane insulating foam. Center: SEM micrograph of such a foam with the struts at the junction of multiple cells highlighted (scale bar is 500 $\mu$m). Adapted with permission from Figure 8 of Xia Cao *et al*. "Polyurethane/clay nanocomposites foams: processing, structure and properties". In: Polymer 46.3 (Jan. 2005), pp. 775–783.©Elsevier 2005 [23]). Right: infrared radiation is mostly absorbed by struts proportional to their cross-sectional area. Therefore, more, smaller struts increases absorption of infrared radiation.

the diameter of the cells (eq 4.10 of [24]). The radiative thermal conductivity is inversely proportional to the extinction coefficient at a fixed temperature (eq 8 of [19]), such that the thermal conductivity would be proportional to the cell diameter according to the model, which is consistent with the empirical result shown in Figure I.5a.

The effectiveness of reducing cell size in reducing the thermal conductivity of RPUFs has typically motivated study on methods for enhancing bubble nucleation [15]. While reducing coalescence and ripening also increases the number density of cells, the desired number density of cells will never be reached without nucleating at least as many bubbles. Bubble nucleation must occur rapidly because each bubble depletes the available dissolved gas in the surrounding medium as it grows. The success of dramatic increases in the nucleation rate in producing foams with more and smaller cells has been demonstrated in nanocellular foams, which are discussed in the next section on $CO_2$-blown foams. Nanocellular foams have so far only been produced in thermoplastic foams by dissolving blowing agent (typically $CO_2$) into the polymer at high pressures (up to 30 MPa) and depressurizing quickly to drive rapid nucleation of bubbles [21]. The production of polyurethane foams, however, is far more complex.

The production of polyurethane foam is a finely tuned symphony of chemical reactions, phase changes, volume changes, and rheological changes. Polyurethane foam is produced by mixing two reacting streams. One stream is predominantly

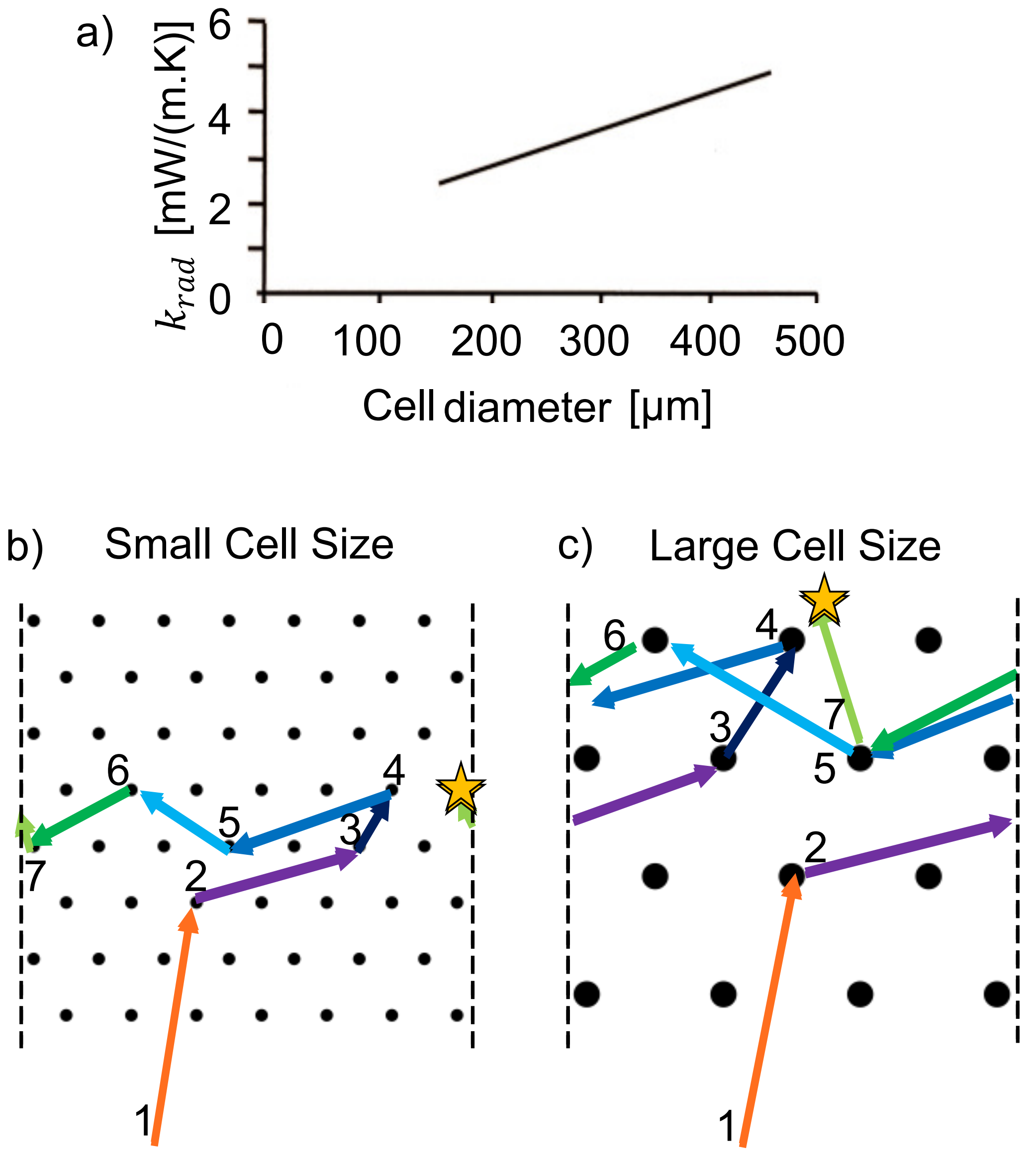

Figure I.5: a) The contribution to the thermal conductivity of a polyurethane foam by radiative heat transfer $k_{rad}$ decreases with the cell size for cells on the order of 100–1000 $\mu$m. Adapted from Figure 15-6 of *The Polyurethanes Book* edited by David Randall and Steve Lee (2002). Made available by the US EPA Health & Environmental Research Online (HERO) database, HERO ID 4159100. b) Schematic of a possible path of an infrared photon through a foam, where each dot represents a strut that can absorb the photon and re-radiate it in a random direction. c) Schematic of the same sequence of absorptions and re-radiations of the photon in (b) but in a coarser foam. The larger spacing between struts allows the photon to travel through the foam more quickly, leading to a higher thermal conductivity through radiation.

polyol, a generic term for a polymer with hydroxyl groups at the end. The polyol is mixed with water, a “physical blowing agent” (PBA), surfactants, flame retardant,

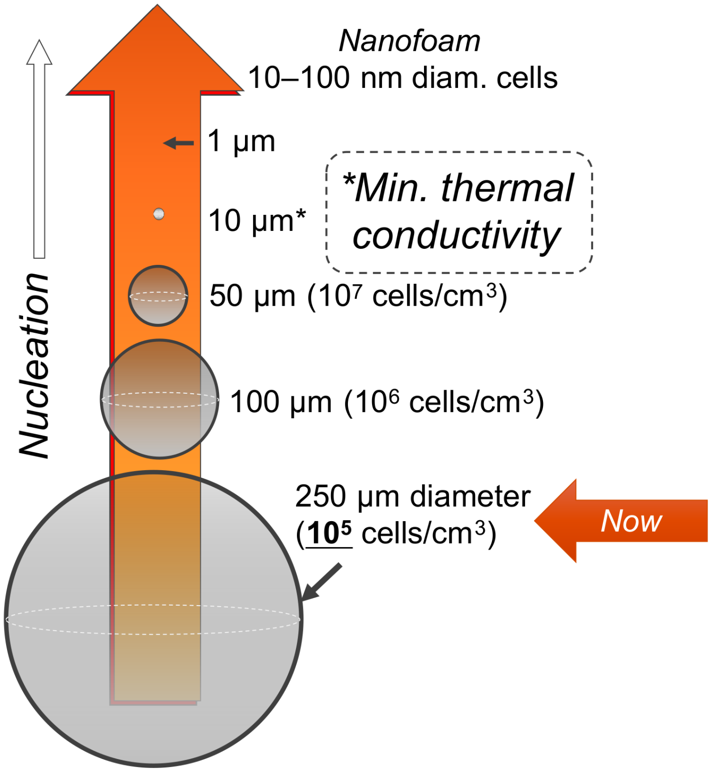

Figure I.6: Schematic of reduction in cell size needed to make significant reductions in the thermal conductivity of polyurethane foams. Current foams have cells of diameter ~ 250 $\mu$m. By reducing the cell diameter to 50 $\mu$m, the overall contribution to the thermal conductivity could be reduced by half (extrapolate trend in Figure I.5). Reducing the cell size by a factor of 5 requires increasing the number of cells by a factor of 125, which will inherently require more bubble nucleation. Note that further reduction in the cell size to the nanoscale would cause radiative heat transfer to increase, but would limit gas conduction by entering the Knudsen diffusion regime.

and catalysts [25]. These components can be mixed together because they are not particularly reactive. The other stream is made purely of isocyanate; nothing is mixed with it due to its highly reactive cyanate end groups. The two streams are mixed at high pressure due to their high viscosities (up to ~ 1 Pa.s). For a discussion of the components of a polyurethane rigid foam, see the patent application by Golini and Guandalini [26].

Once mixed, these two streams undergo two chemical reactions (Figure I.9). The highly reactive cyanate end groups of the isocyanate attack the hydroxyl (-OH) end groups of the polyol to form polyurethane cross-links. The cyanate end groups also react with the hydroxyl groups in the water, which produces carbon dioxide and an amine that then reacts with an isocyanate group to form a urea cross-link. This liberated $CO_2$ drives early blowing of the foam. Later, the heat released from these two exothermic reactions vaporizes the volatile PBA, typically a hydrocarbon like cyclopentane or, historically an HCFC (see discussion on their discontinued use in the next section on $CO_2$-blown foams). For example, the boiling point for cyclopentane, a PBA commonly used in RPUFs, is about 49 °C, while the PU foam can reach 120 °C [25] to 190 °C [7] during curing, lasting minutes to hours. The nucleation of bubbles therefore is driven by an increase in the concentration of gas ($CO_2$ and vaporized cyclopentane) and decreased solubility in the polymer matrix, due to both the rising temperature and curing. Surfactants reduce the interfacial tension of bubbles, decreasing the nucleation barrier (see discussion of the role of interfacial tension in Section I.4) and reducing the driving force for coarsening through coalescence and ripening. The selection of surfactant can mean the difference between an open-cell and a closed-cell foam. Catalysts accelerate the polyurethane synthesis reaction so the foam cures fast enough to prevent collapse, but slowly enough to allow for expansion [7].

When first ejected from the nozzle, the mixture of polyol and isocyanate is still translucent because it has not yet reacted and few bubbles have nucleated. After about 10 seconds, enough bubbles nucleate and grow to micron size that the mixture becomes opaque and has a yellowish, creamy appearance; this point in time is known as the “cream time.” After about 1 minute, the foam becomes sticky, such that inserting and removing a probe (*e.g.*, wooden tongue depressor) leaves a string of foam stuck to the end; this time is known as the “gel time.” Finally, after a few minutes the surface of the foam is no longer tacky, such that a probe does not stick when tapped on the surface; this time is known as the “tack-free time.” Nevertheless, the reaction may continue for hours thereafter [7]. The height and temperature of the foam is plotted over time in Figure I.7.

With so many components interacting simultaneously during the production of an RPUF, identifying the effects of each component on bubble nucleation is challenging. Many studies have focused on the effect of adding micro- or nano-particles to provide more sites for heterogeneous bubble nucleation [15].

Others have focused on dissolving more blowing agent into the polymer to increase bubble nucleation. Depressurization will then induce a greater supersaturation, reducing the nucleation barrier (see discussion of the effect of supersaturation on the nucleation barrier in Section I.4) and increasing the nucleation rate. By

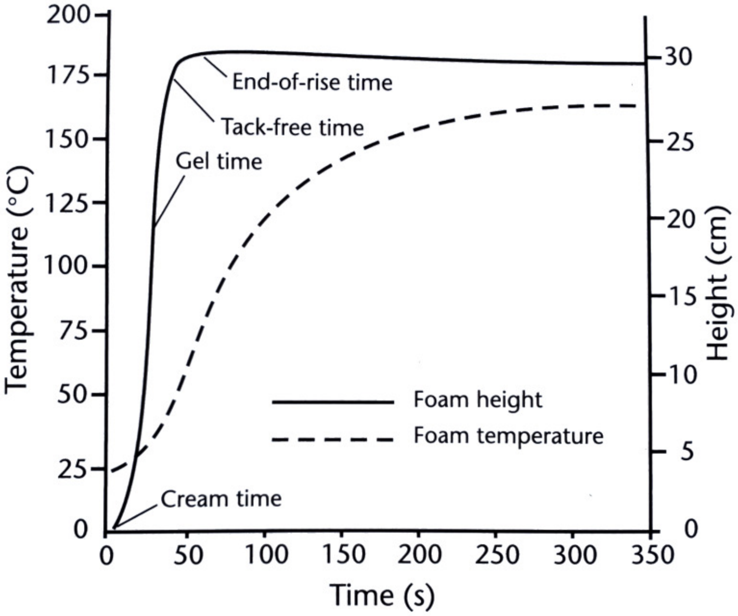

Figure I.7: Polyurethane foam temperature (dashed line, left vertical axis) and rise height (solid line, right vertical axis) over time. The cream time (when the foam becomes opaque), gel time (when the foam becomes sticky and elastic upon poking with a wooden stick), tack-free time (when the foam does not leave a tacky residue upon poking with a wooden stick), and end-of-rise time (when the foam stops rising) are marked. Adapted from Figure 15-1 of *The Polyurethanes Book* edited by David Randall and Steve Lee (2002). Made available by the US EPA Health & Environmental Research Online (HERO) database, HERO ID 4159100.

dramatically increasing the solubility of $CO_2$ in poly(methylmethacrylate) (PMMA) by reducing the saturation temperature to as low as -30 °C [27] or increasing the saturation pressure as high as 30 MPa [22], the average cell size of the resulting foam after a pressure quench can be made as low as 200 nm [22, 28]. Other techniques for enhancing bubble nucleation in polymer foams changes the pressure during the chemical reaction. Simply dropping the pressure more rapidly can increase the nucleation rate of $CO_2$-blown polymer foams by an order of magnitude [29].

Increasing bubble nucleation in reactive foams, such as polyurethane, can be more challenging than in thermoplastic foams due to the dynamic changes in the viscosity and modulus of the polymer during the reaction. Two groups have demonstrated that changing the pressure in specific ways during the chemical reaction can significantly increase bubble nucleation rates. Yang *et al.* described a two-step pressurization process in which the reactants are first saturated with $CO_2$ before the reaction, and then, while the reaction is occurring, the pressure is further increased and held before a rapid depressurization drives foam formation. They found that the curing reaction reduced the solubility of $CO_2$ in the polymer matrix, causing premature bubble nucleation before the pressure quench. By increasing the $CO_2$ pressure during the curing reaction, they found that the resulting foam had micron-sized cells of uniform distribution, which they believe resulted from the suppression of premature bubble nucleation during curing by the higher pressure [30]. Brondi *et al.* described a processing protocol in which the reactants are first saturated with $CO_2$ and the pressure is suddenly quenched partially when the reaction begins. This initial partial pressure quench nucleates many small bubbles but prevents them from growing while the foam is not cured. As the reaction proceeds and the polyurethane foam cures, the pressure is gradually decreased, such that the toughening of the solid matrix matches the added stress from the expanding bubbles to produce a fine-celled foam with minimal coalescence [31].

Due to the difficulty of observing foaming *in situ*, these studies tend to focus on the correlation between the particles added and the foam produced. In this thesis, we seek to address the challenge of direct observation of bubble nucleation in RPUFs. Relative to thermoplastic foams (see Section III.1), observing bubble nucleation in RPUFs is more challenging due to the opacity that arises during the initial mixing of polyol and isocyanate. Direct observation of bubble nucleation during polyurethane foaming has consequently not yet been demonstrated in the literature. Nevertheless, several researchers have made impressive contributions to the understanding of the effects of the compounds and processes involved in polyurethane foaming on bubble nucleation and growth in the last two decades. Minogue is recognized as having published the first live images of bubble growth in polyurethane foam in 2000 [32]. To observe bubbles under a microscope, Minogue first mixed the components of polyurethane with a turbine mixer, then placed a droplet of the mixture on a microscope slide with a spatula and covered it with a coverslip. Despite the potential for inconsistencies in the sample preparation, Minogue repeated each experiment 10 times, which was sufficient to show statistically significant differences between bubble nucleation and growth rates upon the addition of various components of polyurethane, including surfactants, catalysts, and different blowing agents, specifically, cyclopentane and perfluorohexane. The images acquired by this technique are limited in three important ways, however. First, clear images cannot be acquired until about 30 seconds after mixing due to cloudiness resulting from the poor miscibility of polyol and isocyanate. Second, optical microscopy cannot directly observe bubble nucleation because bubble nuclei are smaller than the diffraction limit of light (about 1 $\mu$m). Third, the microscope is focused on the inner surface of the coverslip, so only bubbles that nucleate and grow along this surface are in focus.

Reignier *et al.* [33] overcame these challenges by observing snapshots of bubble growth in PU with cryo-SEM. After mixing the components in a rotating mixer at 2500 RPM, they poured the sample at the desired time into an SEM specimen holder kept cold enough to cryogenically freeze the foam. The morphology of the frozen foam could then be analyzed with SEM. With this freezing technique, they showed the structure of the foam as early as 13 seconds after mixing. Additionally, because the resolution of SEM is much smaller than optical microscopy (order tens of nanometers) due to the shorter wavelength of electrons than optical photons, they could resolve bubbles smaller than 1 $\mu$m. Finally, they could section the frozen sample to examine bubbles that were not affected by the walls of the foaming container. Their unique approach to observing bubbles in the production of RPUFs revealed nanodroplets (14–71 nm in diameter) composed of their PBA (isopentane) dispersed throughout the polymer matrix, which they attributed to emulsification by the surfactant (polysiloxane-ether). They did not observe these nanodomains of PBA in foams frozen more than 24 seconds after mixing, when the temperature had only reached 31.5 °C, while the boiling point of isopentane is only slightly lower (27.8 °C). At this stage of foaming, the number of cells observed was the same as the number of air bubbles entrained during the initial mixing (air bubbles could be clearly distinguished from nanodomains of PBA by their significantly larger size). This observation led them to conclude that the cells they could observe in the final foam were produced by entraining air and not homogeneous bubble nucleation. Their conclusion highlighted the importance of preventing the entrainment of air for the measurement of homogeneous bubble nucleation.

Brondi *et al.* provide a possible explanation for the limited role of $CO_2$ and the PBA in driving bubble nucleation observed by Reignier *et al.* They analyzed bubble growth along an optically clear window inserted into the wall of the foaming container following a procedure similar to the standard cup-foaming procedure (ASTM D7487 [34]). While their observations were limited to bubbles that grew along the optically clear window, they could draw qualitative comparisons between the effects of different processing conditions on the overall nucleation and growth rates of bubbles. They first observed that the number of bubbles decreased in foams produced by mixing at rates fast enough to entrain air bubbles (1000 RPM), suggesting that no new bubbles nucleated while some air bubbles merged. This observation is consistent with the observation of Reignier *et al.* that new bubbles do not nucleate during polyurethane foaming in the presence of entrained air bubbles [33]. When they mixed the foam at a rate slow enough *not* to entrain air bubbles (50 RPM), however, they saw bubbles nucleate. Industrial mixers used for polyurethane are designed not to entrain air, which is a quality that we sought to replicate in our apparatus given the significant effect of entrained air observed in this work by Brondi *et al.* (see Section III.2). This observation suggests that, at least in the presence of a surfactant, liberated $CO_2$ or vaporized hydrocarbon PBA can nucleate bubbles, contrary to the conclusion of Reignier *et al.* [33]. They also observed that foams with cyclopentane (hydrocarbon PBA) in addition to water produced more, larger bubbles than foams without cyclopentane. Minogue also observed that polyurethane foams blown with cyclopentane increased cell size, attributing the improved mixing due to the lower viscosity as the cause [32].

All the previous studies but that of Reignier *et al.* were limited to observation of bubbles that grew along a solid surface. While Reignier *et al.* were limited to interior bubbles frozen at specific times during foaming, Perez-Tamarit *et al.* achieved live imaging of interior bubbles using X-ray tomography [35]. By focusing their observation on bubbles that nucleated in the bulk rather than on those that nucleated heterogeneously on the surface of the container walls, they could more precisely investigate the effect of adding nanoparticles on bubble nucleation. With a time resolution of 156 ms, they showed that adding 3 % by weight of fumed silica nanoparticles (10–40 nm diameter at a density of 60 g/L, or approximately $10^{17}$ particles/cm$^3$) increased the number of bubbles by two orders of magnitude. A similar effect has been observed in a $CO_2$-blown polystyrene foam upon the addition of $10^9$/cm$^3$ talc microparticles (1.8 $\mu$m diameter) to the polystyrene [29]. Nevertheless, published industrial formulations do not include any solid particles [26], suggesting that other disadvantages of adding solid particles might outweigh the advantage of increasing bubble nucleation.

Roberts *et al.* observed foaming in a transparent column after injection of the mixed polyurethane components with a syringe [36]. They observed the foam with three techniques: (1) optical microscopy, (2) SEM, and (3) diffusing wave spectroscopy (DWS). Optical microscopy provided live measurements of the bubble size distribution, but was limited to bubbles that grew along the observation window, as in many of the previous studies discussed above. They referred to this region of the foam as the "skin." SEM provided a high-resolution measurement of the final bulk foam morphology. They noted that the bubbles in the skin observed with optical microscopy had a significantly different size distribution than bubbles in the bulk observed with SEM. To provide live measurements of the bubble size in the bulk, they developed an apparatus to probe the bulk of the foam with a laser and perform DWS on the signal to estimate the average bubble size. Unlike the optical measurements of bubbles along the skin, the DWS measurement of the average size of bubbles in the bulk was consistent with SEM measurements of the final size distribution, providing further evidence of the difference in growth of bubbles along the skin and in the bulk.

A striking visual depiction of this difference is shown for the foaming of polystyrene with $CO_2$ and $N_2$ gas in Figure I.8 [37]. Images are shown before (first image) and after depressurization, with the time since beginning depressurization listed below each image. The region outside the ring is in contact with a surface while the region inside is only exposed to gas, so the bubbles observed within the ring are far more likely to have nucleated in the bulk. Bubbles along the skin are more numerous and larger than bubbles in the bulk.

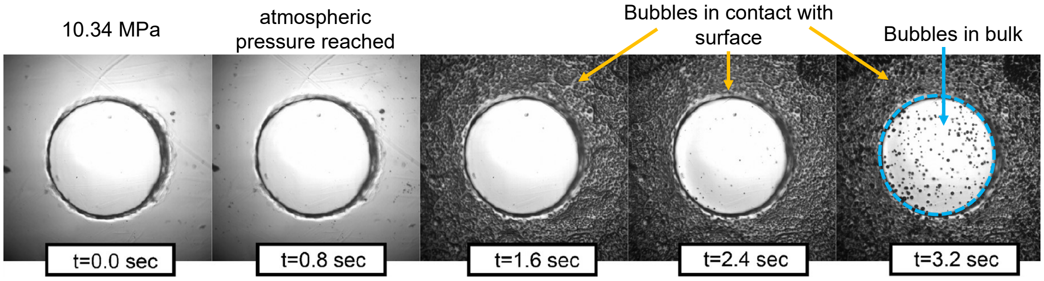

Figure I.8: Nucleation of bubbles in polystyrene blown with a blend of dissolved $CO_2$ and $N_2$ is significantly greater where the polystyrene is in contact with a solid surface than where it is only in contact with the atmosphere (inside blue dashed circle in rightmost image). Adapted with permission from Anson Wong *et al.* “The synergy of supercritical CO2 and supercritical N2 in foaming of polystyrene for cell nucleation”. In: *Journal of Supercritical Fluids* 90 (2014), pp. 35–43. ©Elsevier 2014 [37].

Each of the studies discussed above has made a significant contribution to the general understanding of bubble nucleation and growth in polyurethane foams. The instruments used in each have distinct features, the most important of which are summarized in Table I.1. In entering this field, we identified three features missing from all previous studies, performing a continuous foaming process and imaging within 100 ms from the start of foaming, and producing foam from a high-pressure nozzle, which are written in bold in the Table. The first, continuous foaming, is important because much more data can be collected from a continuous process than a batch process. The second, imaging within 100 ms from the start of foaming, is important because the initial degree of mixing of the polyol and isocyanate has been shown to affect the foam structure. The third, producing the foam from a high-pressure nozzle, is important for making a more direct comparison to industrial foaming, where RPUFs are produced from nozzles at pressures exceeding 8 MPa [16]. In many extruded foams, bubbles may nucleate within the nozzle because the pressure will decrease below the saturation pressure of the dissolved gas. If too many bubbles form in the nozzle, they may expand too rapidly as a result of the large decrease in pressure upon exiting the nozzle and lead to some collapse of the foam [38], but bubble nucleation in a nozzle has not yet been reported in the literature. We therefore designed the instrument for the present study to provide these features (see Chapter III).

| Feature | [32] | [35] | [33] | [39] | [36] | This work |
|---|---|---|---|---|---|---|
| Can measure bubbles in the bulk |  | ✓ | ✓ |  | ✓ | ✓ |
| Live imaging | ✓ | ✓ |  | ✓ | ✓ | ✓ |
| Sub-micron imaging |  |  | ✓ |  | ✓ |  |
| 3D imaging |  | ✓ |  |  |  |  |
| Images bubbles 1–90 s after mixing | ✓ | ✓ | ✓ | ✓ | ✓ |  |
| Images bubbles > 90 s after mixing | ✓ |  |  | ✓ | ✓ |  |
| Prevents entrainment of air | ✓ |  |  | ✓ |  | ✓ |
| **Continuous process** |  |  |  |  |  | ✓ |
| **Images within 100 ms from start of foaming** |  |  |  |  |  | ✓ |
| **Foam produced in high-pressure nozzle** |  |  |  |  |  | ✓ |

Table I.1: Compares key features of studies of polyurethane foaming by previous research groups with the present work. Unique features of the experimental method described in the present thesis are bolded. Studies are listed by reference number in the table. Author list and year for each study are listed here: [32] Minogue (2000), [35] Perez-Tamarit *et al.* (2019), [33] Reignier *et al.* (2019), [39] Brondi *et al.* (2021), [36] Roberts *et al.* (2022).

In addition to developing an instrument capable of achieving those three features, the present work aimed to elucidate the specific role of the many components of the polyurethane formulation. Therefore, rather than study a full formulation, we

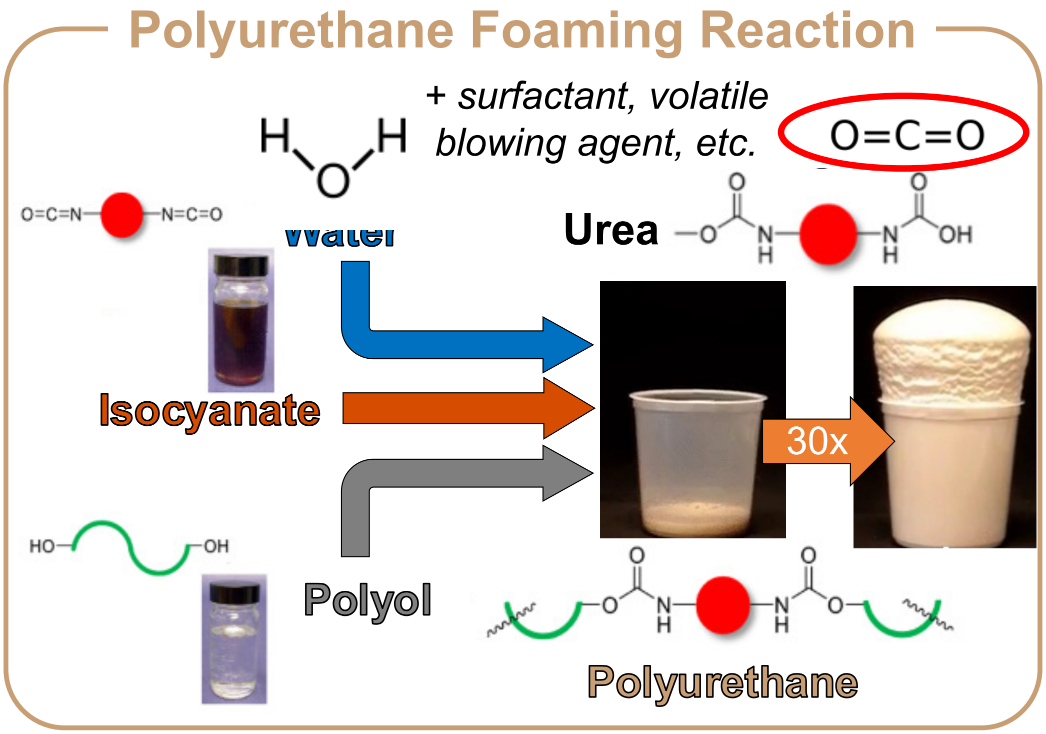

Figure I.9: Schematic of the polyurethane reaction, focusing on the main chemical reactions (polyol + isocyanate to form polyurethane and isocyanate + water to form $CO_2$ and urea). The foam also usually has surfactants and volatile blowing agents (*e.g.*, cyclopentane) mixed in the polyol formulation. The polyurethane foam can grow in volume by a factor of 30, as shown schematically by the beginning and end of a cup foaming experiment shown in the center (to expand by a factor of 30, foam must be produced in a high-pressure nozzle). Molecular structures and macroscale pictures of chemicals used with permission from Dr. Chris Letko of Dow, Inc. Original source for cup foaming experiment unknown.

began with the simplest model system for polyurethane, polyol and $CO_2$, shown in Figure I.10. Polyol and $CO_2$ were selected to be the model system given their ability to produce a foam with a similar expansion ratio and viscosity (prior to curing) as polyurethane. Due to the technical difficulty of generating carbon dioxide *in situ*, we study bubble nucleation from carbon dioxide dissolved in the polyol inside a high-pressure reactor. This mixture is then transferred under pressure to a high-pressure syringe pump for use in our experimental apparatus (presented in Chapter III). While this method of bubble nucleation is more similar to $CO_2$-blown foams like polystyrene (see discussion of these foams in the next subsection) than foams with $CO_2$ produced *in situ* like polyurethaen, we believe that its study will provide a foundation for individually studying the effects of each of the key components in a polyurethane formulation: PBA, surfactant, isocyanate, heat, water, and catalyst.

Due to the complexity of the experiment, we have only just begun investigation into the effects of adding either cyclopentane (PBA) or surfactant, as discussed in Chapter VII.

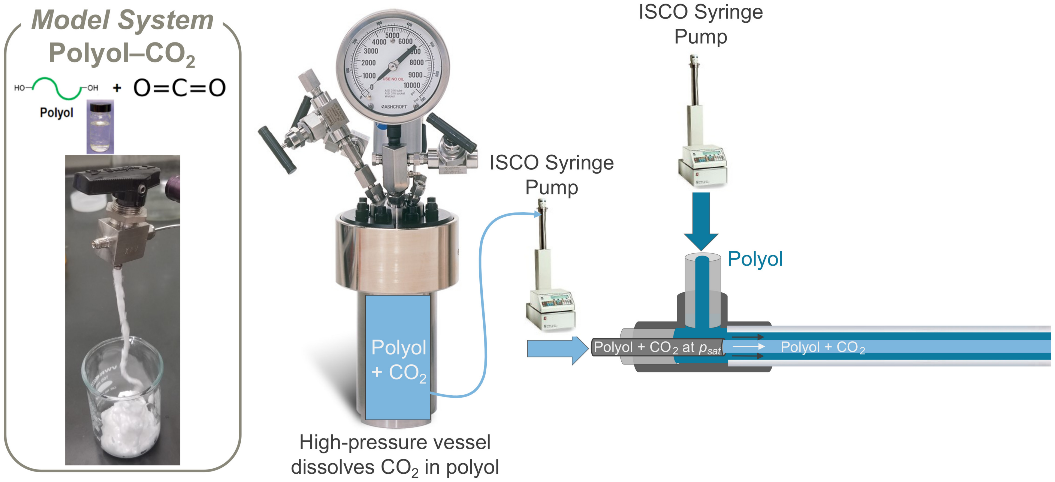

Figure I.10: Schematic of model system of the fewest components required to make a convincing foam: polyol and $CO_2$. Experimental procedure shown to the right. Because of the absence of isocyanate and water, $CO_2$ is not produced in the model system, so it is instead dissolved into polyol under high pressures in a Parr reactor. The mixture is then transferred under high pressure to an ISCO syringe pump, which pumps it into the inner stream of the microfluidic channel used to study bubble nucleation (discussed in Chapter III—see Figure III.1). Additional components can be added in sequentially to understand their effect on bubble nucleation and growth. Molecular structures and macroscale pictures of chemicals used with permission from Dr. Chris Letko of Dow, Inc. Original source for cup foaming experiment unknown.

Polyols used in polyurethane are typically either polyether polyols or polyester polyols. In general, polyether polyols are chosen for thermally insulating polyurethane foams because of their hydrolytic stability [40], easier processability (liquid at room temperature), and highly customizable architecture relative to polyester polyols [40]. Most RPUFs are produced with polyether polyols of high functionality, meaning a high number of hydroxyl functional groups per polymer chain, which yields a greater number of cross-links for a more rigid foam [7]. For these reasons, we will focus on polyether polyols in the present work, using higher functionality polyols where possible.

In Chapter VII, we explore the effects of adding other ingredients in the polyurethane formulation, specifically, cyclopentane (physical blowing agent) and silicone surfactant. While most who have worked with polyurethane observe that the properties of polyurethane cannot be extrapolated based on the individual effects of each component, we hope that by carefully measuring the effects of individual components on bubble nucleation and comparing to theoretical models, we provide useful insights into the roles played by each component in achieving the remarkable properties of polyurethane insulating foams.

### Carbon Dioxide: The Green Option for Blowing Foams

Foams blown with $CO_2$ are valuable for their lower impact on the environment. In the late 1950s, manufacturers discovered that they could produce polyurethane foams with unprecedented low thermal conductivity by blowing with chlorofluorocarbons (CFCs) in addition to the $CO_2$ produced from the reaction of isocyanate and water. CFCs have half the thermal conductivity of $CO_2$ (7.4 mW/(m.K) for CFC-11 ($CCl_3F$) vs. 15.3 mW/(m.K) for $CO_2$ at 10 °C) due to their slower diffusivity resulting from their higher molecular weights (137.4 g/mol for CFC-11 ($CCl_3F$) vs. 44 g/mol for $CO_2$), as shown in Figure I.11 [7]. CFCs also deplete the ozone and were phased out over a decade ago according to the 1987 Montreal Protocol [7].

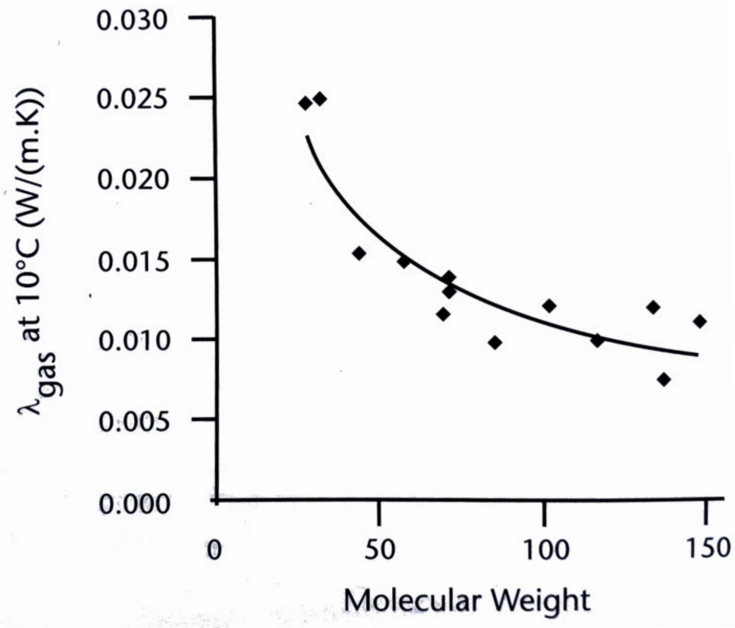

Figure I.11: Thermal conductivity contribution from gas conduction $\lambda_{gas}$ plotted as a function of the molecular weight of different physical blowing agents. Data are plotted as diamonds and a curve is drawn to guide the eye. Reproduced from Figure 15-8 of *The Polyurethanes Book* edited by David Randall and Steve Lee (2002). Made available by the US EPA Health & Environmental Research Online (HERO) database, HERO ID 4159100.

Following the adoption of the Montreal Protocol, hydrochlorofluorocarbons (HCFCs) were introduced as alternatives to CFCs due to their significantly lower ozone depletion potential, but because they nevertheless deplete the ozone and typically have a global warming potential one thousand times larger than that of $CO_2$, they are planned to be phased out by 2040 according to the 1992 Copenhagen amendment to the Montreal Protocol [7]. Hydrofluorocarbons (HFCs) are currently used as alternatives to CFCs and HCFCs because their lack of chlorine means that they do not deplete the ozone and research suggests that they do not contribute to smog [7]. They nevertheless have a global warming potential of about a thousand times more than $CO_2$ (1600 for HFC-134a vs. 1 for $CO_2$), but are targeted for phasing out by the Paris Climate Agreement (2015) and the Kigali amendment to the Montreal Protocol (2016) [41]. Hydrocarbons, particularly isopentane and cyclopentane, emerged as alternative physical blowing agents in the late 1980s with the development of technology for safe handling of these flammable compounds during manufacturing [7]. Nonetheless, foams blown with hydrocarbons pose a high risk of flammability to customers, even with the addition of flame retardants [42]. Perfluorocarbons (*e.g.*, $C_5F_{12}$) are non-flammable alternatives to hydrocarbons, but due to their high global warming potential, they have not been used in commercial polyurethane foams [7].

In contrast, $CO_2$ poses none of the hazards caused by the blowing agents listed above: it does not deplete the ozone, it is not flammable, and it has a negligible global warming potential because the $CO_2$ feedstock often comes from industrial waste streams that would otherwise end up in the atmosphere. Nitrogen gas $N_2$ is also a sustainable blowing agent, but it is less commonly used due to lower solubility in many polymers [43, 44] and higher interfacial tension [44], which may hinder nucleation. It is worth noting, however, that a 75:25 mixture of supercritical $CO_2$ and supercritical $N_2$ can yield a higher cell number density in polystyrene foaming as compared to either pure gas in its supercritical state [37].

Were blowing high-quality foams easier with $CO_2$ than CFCs, we never would have gone through the trouble of synthesizing CFCs. CFCs, however, are highly soluble in a variety of polymers at atmospheric pressure, while $CO_2$ requires several MPa of pressure to reach even 10% solubility (see Chapter II). Closed-cell foams filled with CFCs also have lower thermal conductivity, due to both the lower thermal conductivity of CFC than $CO_2$ mentioned above and the lower diffusivity of CFCs, which slows the rate that the blowing agent diffuses out of the foam [45]. Due to the higher thermal conductivity of $CO_2$ gas resulting from its lower molecular weight, thermal conductivity must be reduced through structural improvements, in particular, increasing cell density and expansion ratio. Previous studies have shown that both of these properties increase with the amount of dissolved $CO_2$ [22, 28, 46]. Furthermore, the accessibility of the supercritical regime of $CO_2$ (> 7.39 MPa, > 31.6 °C [47]) made possible the development of microcellular foams due to its low interfacial tension that promotes bubble nucleation [30] (see discussion of role of interfacial tension in nucleation in Section I.4). $CO_2$ also acts as a plasticizer that can allow for easier processability and extrusion [48].

Foams blown with $CO_2$ are produced in two stages. First, $CO_2$ must be dissolved into the glassy polymer by pressurizing the atmosphere with $CO_2$ to several MPa, making it easier to process by lowering the glass transition temperature $T_g$ below the processing temperature. Second, the foam is expanded. The polymer is initially expanded by reducing the pressure, but glassier polymers with higher $T_g$ may be subsequently heated for further expansion. The resulting foam ultimately solidifies as the polymer cools and loses dissolved $CO_2$, returning it to its glassy state [49].

Often, foams blown with $CO_2$ are lower in performance and more challenging to produce than foams blown with other blowing agents. The production of $CO_2$-blown foams with properties competitive with other commercial foams requires that the foam be made microcellular, meaning that the cell size must be on the order of 1–100 $\mu$m [50]. Producing microcellular foams requires a large enhancement in nucleation only possible with supercritical or liquid $CO_2$, due to the reduction in interfacial tension along the surface of bubble nuclei (see Section I.4 for a discussion of the role of the interfacial tension in the nucleation rate). The high pressures needed to use supercritical and liquid $CO_2$ require more robust equipment and additional safety protocols, which add to the cost. Furthermore, before blowing a foam with $CO_2$, the $CO_2$ must be dissolved into the polymer, which may take on the order of days even for a 1.5 mm-thick sample [51]. Consequently, few $CO_2$ blown foams exist commercially, although they are replacing the more hazardous and environmentally harmful blowing agents listed above in some foams, such as polystyrene coffee cups and meat trays. More often, $CO_2$ is effective as a co-blowing agent, as in the case of polyurethane and structural polystyrene foams, where $CO_2$ is mixed with volatile hydrocarbons [45].

Should the cost of blowing polymer foams with supercritical $CO_2$ be made economical, it may provide a feasible route to the production of nanocellular foams. Nanocellular foams are foams with cells that are significantly smaller than 1 $\mu$m, often with the goal of producing cells smaller than 100 nm to reach a new regime of thermal, dielectric, mechanical, and optical properties [52]. They require substantially more bubble nucleation, which is made possible by (1) dissolving high concentrations of $CO_2$ (> 25%) into the polymer, often requiring high pressure (*e.g.*, > 20 MPa) and low temperature, (2) quenching the pressure fast enough that the $CO_2$ remains supercritical and avoids the high nucleation barrier of the liquid–vapor equilibrium, and (3) adding nanoparticles to act as nucleation sites [53]. Nanocellular foams are particularly relevant to primary application of the present work, the reduction of the thermal conductivity of insulating foams, having a cell size smaller than the mean free path of air. When gas molecules are confined to dimensions smaller than their mean free path, they no longer conduct heat as efficiently, being frequently interrupted by the confining structure. This reduction in heat conduction is known as the “Knudsen effect,” and is the same mechanism by which aerogels have such low thermal conductivity as well [52].

Every nanofoam relies on a substantial increase in bubble nucleation relative to microfoams because the number density of cells grows as the inverse third power of the cell size. While many techniques have been shown to enhance bubble nucleation enough to produce reliable nanofoams, from applying a stress to reduce the nucleation barrier energy [54] to inducing nanoscopic phase separation with block copolymers [55], nanofoams still have a relatively lower porosity (maximum 85% [52]) than commerical polyurethane foams [7]. Therefore, while the gas component of nanofoams may have a lower thermal conductivity than polyurethane foams, its solid component conducts significantly more heat. Greater porosity is necessary to make nanofoams commercially viable.

## I.4 Bubble Nucleation: Many Models, Few Measurements

Bubble nucleation inherently takes place out of equilibrium when a liquid is brought to a metastable state in which a vapor phase is more thermodynamically stable. Therefore, a rigorous treatment of bubble nucleation would employ a kinetic model [56]. A proper kinetic model of bubble nucleation considers bubble embryos consisting of 1, 2, 3,..., $N$ particles, where $N$ is some number much larger than the smallest stable nucleus, defined by the critical radius. A particle may enter an embryo, increasing its size by 1, or it may leave, decreasing its size by 1, with the rate of each depending on the nucleus size and supersaturation. Most embryos are unstable and dissolve back into solution, but those that reach a critical size continue to grow according to the transport properties of the medium. Modeling this kinetic process therefore requires both (1) molecular precision to resolve absorption and desorption of single molecules and (2) long simulation times for representative statistics of the frequency of successful bubble nucleation. Molecular dynamics simulations have successfully estimated homogeneous bubble nucleation rates in single-component vapors under high supersaturation, for which the critical embryo size is small and nucleation rate is high [57].

To identify the "onset" of nucleation, *i.e.* the supersaturation at which bubbles nucleate within a time scale relevant for experimental observation (typically seconds), a more efficient calculation is required. In these cases, the supersaturation is small, such that the critical size of the bubble embryo is large enough to be treated as a uniform thermodynamic phase. Furthermore, bubble nucleation is rare enough that it is limited by the reversible work $\Delta G^*$ required to form a bubble embryo of the critical size. Therefore, if we assume a well-defined interface and constant temperature during nucleation—which are not guaranteed for the nucleation of a vapor in a liquid—the nucleation of a bubble can be approximated as a quasi-equilibrium process where the rate of nucleation $J$ is proportional to the Boltzmann factor corresponding to the critical embryo size

$$J \propto e^{-\Delta G^*/k_B T} \tag{I.1}$$

This Arrhenius-like model for bubble nucleation was first proposed by Volmer and Weber [58] using the thermodynamic principles of Gibbs and Boltzmann [59]. The full development of the thermodynamic model of bubble nucleation into a formalized theory, known as "classical nucleation theory" (CNT), including the derivation of the prefactor for the exponential term based on the conditions of the system and deviations from equilibrium, are credited to Farkas [60], Kaischew and Stranski [61], Becker and Döring [62], Zeldovich [63], and Kagan [64]. Their work showed that the thermodynamic picture of bubble nucleation that is the hallmark of CNT emerges from the application of constraints to the kinetic model. Assuming that the metastable state is stable enough for the sizes of bubble embryos to reach an equilibrium distribution and that the rates at which particles are absorbed into and released from the embryo are independent of time and embryo size and occur one at a time (*i.e.* no merging or splitting of embryos), the rate at which embryos of $n-1$ particles gain a particle and grow to size $n$ is equal to the rate at which embryos of

$n$ particles lose a particle and shrink to size $n-1$ by microscopic reversibility. This assumption is the key to reaching a thermodynamic model from a kinetic framework because it allows the use of Boltzmann factors to estimate the number density of embryos of different sizes. The Boltzmann factor, $e^{-\Delta G(n)/k_B T}$ requires the calculation of the reversible work $\Delta G(n)$ to form an embryo of $n$ particles. Due to the small size of the embryos, the application of thermodynamics is not always appropriate because it models each phase as a homogeneous bulk. In cases where the critical embryo size is large enough to be described as a bulk thermodynamic phase and the interfacial tension along the surface of the embryo can be well approximated by the planar surface tension, treating the embryo as a uniform thermodynamic phase and its surface as an infinitesimal boundary is reasonable [65].

In this thermodynamic picture, the dominant contributions to the reversible work to form an embryo of size $n$ are the lower chemical potential of the embryo, which is the driving force for nucleation resulting from supersaturation, and the energy penalty for creating a surface between the embryo and the mother phase, which drives the dissolution of the embryo. The first is proportional to the volume and the second to the area.

In the case of a single-component mixture, this thermodynamic picture results in the following equation for the reversible work of embryo formation,

$$\Delta G(n) = (\mu_{bub} - \mu_{bulk})n + F(n)\gamma \tag{I.2}$$

where $\mu_{bub}$ is the chemical potential of the bubble embryo, $\mu_{bulk}$ is the chemical potential of the bulk mother phase, $F(n)$ gives the surface area of an embryo of $n$ particles, and $\gamma$ is the interfacial tension along the surface of the embryo. If we assume that the embryo is a sphere of radius $R$, then $n = \frac{4\pi}{3}R^3 v$ where $v$ is the volume of one particle, and $F(n) = 4\pi R^2$. Letting $\Delta\mu \equiv \mu_{bulk} - \mu_{bub}$, which must be greater than 0 for bubble nucleation, we can rewrite equation I.2 as

$$\Delta G(R) = -\frac{4\pi}{3}R^3 v(\Delta\mu) + 4\pi R^2\gamma \tag{I.3}$$

This expression for the reversible work to form a bubble embryo of radius $R$ is plotted in Figure I.12. Based on this model, the reversible work peaks at a critical radius $R^*$: the drive to lower energy will cause smaller bubble embryos to shrink and larger bubble embryos to grow.

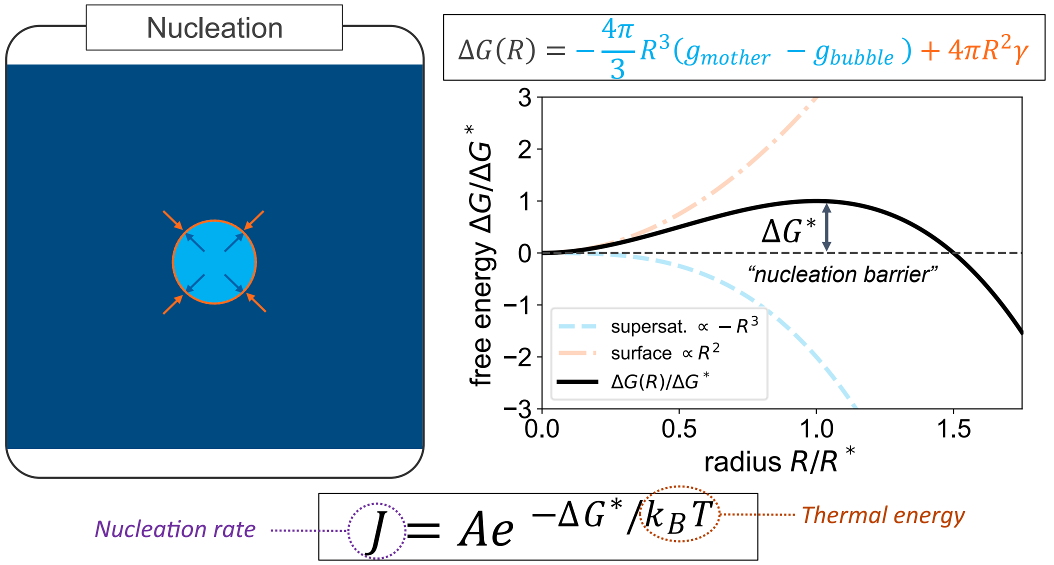

Figure I.12: The reversible work to form a bubble embryo of radius $R$ is plotted (black solid line) alongside the energy gain due to supersaturation proportional to the volume (red dashed line) and the energy penalty due to the formation of an interface proportional to the surface area (blue dot-dash line). The radius $R$ is scaled by the critical radius $R^*$ and the reversible work $\Delta G(R)$ is scaled by the value at the critical radius $\Delta G^* \equiv \Delta G(R^*)$. The maximum value or "nucleation barrier" is indicated with an arrow as $\Delta G^*$.

By maximizing $\Delta G(R)$ with respect to $R$ in equation I.3, the critical radius is found to be

$$R^* = \frac{2\gamma}{v(-\Delta\mu)} \tag{I.4}$$

and the corresponding critical energy, known as the "nucleation energy barrier," is

$$\Delta G^* = \frac{16\pi}{3}\frac{\gamma^3}{v^2(\Delta\mu)^2} \tag{I.5}$$

although for an incompressible bubble assumed to be in equilibrium with the surrounding fluid, the following more convenient and experimentally tractable form of the nucleation barrier can be used [66]:

$$\Delta G^* = \frac{16\pi}{3}\frac{\gamma^3}{(\Delta p)^2} \tag{I.6}$$

where $\Delta p = p_{sat} - p$ with $p_{sat}$ that pressure at which the gas was saturated in the mother phase. While more applicable to the condensation of liquid droplets (the subject of Kalikmanov's review), the formula provides a tractable formula for rough calculations.

Because we have assumed that the size distribution of bubble embryos is given by the equilibrium distribution, which is proportional to the Boltzmann factor for each size $e^{-\Delta G(n)/k_B T}$, there are exponentially fewer bubble embryos of sizes near the critical size with radius $R^*$. This minimum in the bubble population creates a bottleneck in the kinetic picture: there are so few bubbles of this size that the rate of bubble nucleation is almost entirely determined by the rates of growth of bubbles of similar size. In the mathematical derivation, this feature allows an integral (which is used to approximate a summation to high accuracy) to be approximated by the quadratic expansion about the peak at $R = R^*$, which yields an expression for the nucleation rate of the following form

$$J = j(R^*)Z\left[N_{tot}\exp\left(-\frac{\Delta G^*}{k_B T}\right)\right] \tag{I.7}$$

where $j(R^*)$ is the product of the rate at which particles are absorbed into the embryo per unit area and the surface area of the critical nucleus $4\pi(R^*)^2$, originally suggested by Farkas [60], $Z$ is the Zeldovich factor [63], which is proportional to the square-root of the second derivative of the reversible work at the peak $R = R^*$ and gives the deviation of the distribution of embryo sizes from the equilibrium distribution given by the Boltzmann factors [5], and $N_{tot}$ is the total number density of bubble embryos which, when scaled by the Boltzmann factor, gives the rough number of critical bubble embryos. This model ignores the limitations of diffusion, viscosity, and inertia in the bulk fluid. While these aspects of the mother phase do not affect the exponential term, they can affect the form of the prefactor [5]. For further details of the mathematical derivation of this formula from the kinetic picture, see the review articles by Blander and Katz [5] and Oxtoby [67], and the books by Skripov [68], Debenedetti [56], and Kalikmanov [66].

For the experimentalist, the most significant feature of the model for the nucleation rate given in equation I.7 is the strong dependence of the exponential term on the supersaturation, quantified by the difference in chemical potential between the nucleating phase and the mother phase $\Delta\mu$. Because the prefactor tends to have a much weaker dependence on the supersaturation, it can generally be ignored in identifying the onset of bubble nucleation [5]. Therefore, a precise estimate of the nucleation energy barrier $\Delta G^*$ may be sufficient to identify the supersaturation at which bubble nucleation becomes observable.

Because the measurement of the chemical potential is not straightforward, the expression for the nucleation energy barrier given in equation I.5 is often further simplified by making one of the following two assumptions: (1) the fluid is ideal, or (2) the fluid is incompressible. These yield the approximations for $\Delta\mu$ of (1) $\Delta\mu \approx \Delta p$, where $\Delta p$ is the difference in the saturation pressure and the ambient pressure, and (2) $\Delta\mu \approx \log S$, where $S = \frac{p_{sat}}{p_{amb}}$ is the supersaturation ratio of saturation to ambient pressure.

These approximate models can yield reasonable agreement with experimental measurements. The most rigorous validation of classical nucleation theory (CNT) for homogeneous nucleation comes from studies of the superheating of liquids. Skripov reports a variety of early works in which the measured onset temperature of bubble nucleation in superheating liquids differed from the prediction by the appropriate form of CNT by less than 2 °C, which was often within the experimental error of the time [68]. He reasoned that the high sensitivity of the exponential term to temperature yielded a very sharply defined onset. The advantage of superheating water for testing CNT was more recently demonstrated by Ando *et al.*, who utilized a laser to superheat small regions of the bulk of a container of water, such that all nucleation was homogeneous due to the isolation from the container walls. They found that even the onset of bubble nucleation in water can be reasonably described by CNT [69]. Most notably in the field of polymer foaming, Goel and Parks demonstrated reasonable agreement between not just the onset of nucleation but also the nucleation rates observed in foams of poly(methyl methacrylate) (PMMA) and supercritical $CO_2$ [70]. In general, however, CNT tends to perform better for the precipitation of larger molecules, such as polymers in poor solvents, where “even a single chain takes the form of a spherical globule with a fairly uniform core when the chain is long enough” [71].

Nevertheless, CNT has generally faced considerable challenges in modeling nucleation in multicomponent mixtures. While the theory has been extended successfully to multiple components [56, 72], two of the fundamental assumptions of the theory often fail in multicomponent mixtures. First, the concentration profile of the components can be highly non-uniform, violating the assumption by CNT that each phase is homogeneous. In particular, when a volatile compound is dissolved in a liquid, as in the case of polymer foaming that is the focus of the present work, the volatile component tends to aggregate along the surfaces of bubbles due to the gain in attractive energy, as shown by Talanquer and Oxtoby using classical density functional theory (DFT) [65]. This aggregation significantly affects the interfacial tension, which they found to result in errors in the prediction of the nucleation rate by CNT of factors up to $10^{20}$. Xu *et al.* likewise found that the assumption of a infinitesimal interface by CNT yields an incorrect interfacial tension [73]. Second, multicomponent mixtures may nucleate in more than one step, while CNT assumes nucleation is completely defined by the overcoming of a single nucleation energy barrier $\Delta G^*$. This behavior results from the Gibbs phase rule, according to which multicomponent mixtures can access more phases than pure substances. While there are exceptional cases in which CNT provides an accurate model for two-stage nucleation, it generally fails [74]. For example, in some mixtures of liquid and volatile fluid, the critical embryo size is small enough that the aggregation of volatile fluid along the surface may extend deep inside the embryo, such that the density of the embryo is more liquid-like than vapor-like. Consequently, the driving force of supersaturation is much smaller than the difference in chemical potential between the vapor bubble phase and the liquid mother phase assumed by CNT [65].

Both of these problems arise in the case of polymer foams. Due to the high pressures at which blowing agents like $CO_2$ are dissolved in the polymer melt before foaming, the concentration of $CO_2$ in the mixture is high. Furthermore, under fast depressurization, the concentration may be high enough to form a liquid-like bubble before vaporizing. Xu *et al.* predicted such a pathway to bubble nucleation in the case of poly(methyl methacrylate) (PMMA) blown with $CO_2$ [73]. They first corrected the interfacial tension in the CNT model to account for the first issue arising from aggregation of $CO_2$ along the interface, which raised the predicted nucleation barrier. When they fully accounted for the non-uniform, liquid-like concentration profile of $CO_2$ in the bubble using DFT, they predicted a significantly higher nucleation energy barrier than predicted by CNT, even with the corrected interfacial tension. When modeling bubble nucleation in polymer foams, CNT also introduces errors by neglecting the change in conformational entropy of polymer chains along the surface of small, high-curvature bubbles [75]. This error leads to a significant *over*estimate of the nucleation energy barrier. CNT also fails to account for variations in polymer architecture unless they change the bulk properties [76].

CNT tends to fail near the spinodal at high supersaturations, as well. While the CNT formula for the nucleation energy barrier in equation I.5 reaches a plateau as the supersaturation reaches its maximum value (when the chemical potential of the nucleating phase reaches its minimum), the nucleation energy barrier actually drops below the thermal energy $k_BT$ and approaches zero. A more appropriate model of nucleation is given by Cahn and Hilliard [77], which accurately captures the vanishing of the nucleation energy barrier. This model tends to fail for nucleation energy barriers greater than the thermal energy $k_BT$ (see [78]), which are the most relevant to physical polymer foaming processes.

In the intermediate regime between the binodal and spinodal where CNT and Cahn–Hilliard theory fail, more sophisticated models like density functional theory or self-consistent field theory are required [78]. Although molecular dynamics simulations could provide high accuracy estimates of the bubble nucleation rate [57], the computational requirements limit them to short times, so they are more useful for high degrees of supersaturation than for determining the onset of nucleation. Instead, we adopt the approach of Xu *et al.* [73, 79] and model the non-uniform concentration profile of both polymer and dissolved gas using DFT, as first demonstrated by Talanquer and Oxtoby [65]. We then employ the "string method" as a tool to identify the pathway that requires the least addition of free energy [80, 81]. By considering the free energy along the entire path, the string method can identify multi-step nucleation pathways that require less energy than the single-step pathways to which CNT is limited. The string method is still limited in its application because it assumes a quasi-equilibrium is reached at each point along the pathway, which is only valid when nucleation is rare enough that bubble embryos may explore many pathways before nucleating. While the string method has made predictions consistent with experiments in other systems, such as membrane fusion [82], its predictions of bubble nucleation (see [73, 79]) have not been compared against experiments (see Section III.1 for a review measurements of bubble nucleation). In particular, the prediction of two-stage nucleation starting with a liquid–liquid phase separation has not been verified. The present work intends to provide the foundation for such verification. The importance of validating models of bubble nucleation against experimental measurements was underscored in the review by Di Maio and Kiran in 2018, in which they noted that "the current lack of [nucleation's] full understanding presents the main actual limitation to modeling the foaming process" [83]. This lack of understanding motivated the beginning of the present work and has remained throughout its course. In 2022, Roberts *et al.* noted that "models that include the effects of bubble growth have also been developed for PU foams but suffer from a dearth of bubble-scale data" [36]. There are many models, but few measurements. The present work provides a few more.

### I.5 Summary of Contents

This thesis is organized along the lifetime of a bubble. We begin by discussing the source of all bubbles, the mother phase, in Chapter II. Specifically, we present measurements of the thermophysical properties of the polyol–$CO_2$ mixtures prepared as sources of bubble nucleation for the experiments discussed in the rest of the thesis. The measurements were taken using the G-ADSA technique developed by Prof. Ernesto Di Maio at the University of Naples. We also explore the effects of polyol architecture on the solubility of $CO_2$, noting a non-monotonic dependence on the molecular weight. We then describe the microfluidic flow-focusing apparatus through which we flow the mother phase to drive local, reproducible, and continuous bubble nucleation for observation with high-speed microscopy in Chapter III. The image-processing algorithms for analyzing the high-speed microscopy videos are discussed in Chapter IV.

Having described the experimental setup, we present experimental measurements of bubble growth in Chapter V. Because high-speed microscopy cannot directly detect bubble nucleation, we estimate the time of nucleation by fitting a model of bubble growth to measurements and extrapolating its predicted dynamics backward to the critical nucleus size. We compare two models for bubble growth and find that both yield reasonable agreement. We then analyze the statistical distribution of predicted nucleation times through two approaches to demonstrate that the nucleation behaves like homogeneous nucleation, which we then compare to models of homogeneous bubble nucleation in Chapter VI. First, we show that a quantity related to the time between nucleation events at the same degree of supersaturation along the length of the microfulidic channel follows an exponential decay characteristic of a random Poisson process, from which we can estimate a nucleation rate. Second, we count the number of events per time at a particular degree of supersaturation and divide by the volume and time over which the nucleation events were counted, which revealed that the nucleation rate was sensitive to the supersaturation. Both methods measured similar nucleation rates, so we compared their measurements to predictions by a model based on the string method and classical nucleation theory, finding that the string method model could describe the data while the classical nucleation theory could not. Having demonstrated our proposed method for estimating the nucleation rate with supersaturation, we show that adding cyclopentane to a mixture of polyol and $CO_2$ dramatically enhances bubble nucleation in Chapter VII. Using the string method model and measurements of phase behavior, we provide evidence that the cause of the enhanced bubble nucleation is the opening up of a two-stage nucleation pathway with a significantly lower nucleation energy barrier upon the addition of cyclopentane. We also discuss future work for studying the effects of other additives from a full polyurethane foaming reaction missing from our model system. Finally, we present a survey of observations of what happens after bubbles grow too large for the nucleation analysis in Chapter VIII, exploring the dynamics of bubbles when they grow so large that they elongate, ripening and coalescence of bubbles, and flow instabilities.

Throughout the thesis, we complement theory and experiment to arrive at a deeper understanding of bubble nucleation. The roadmap we followed to arrive there is shown in Figure I.13.

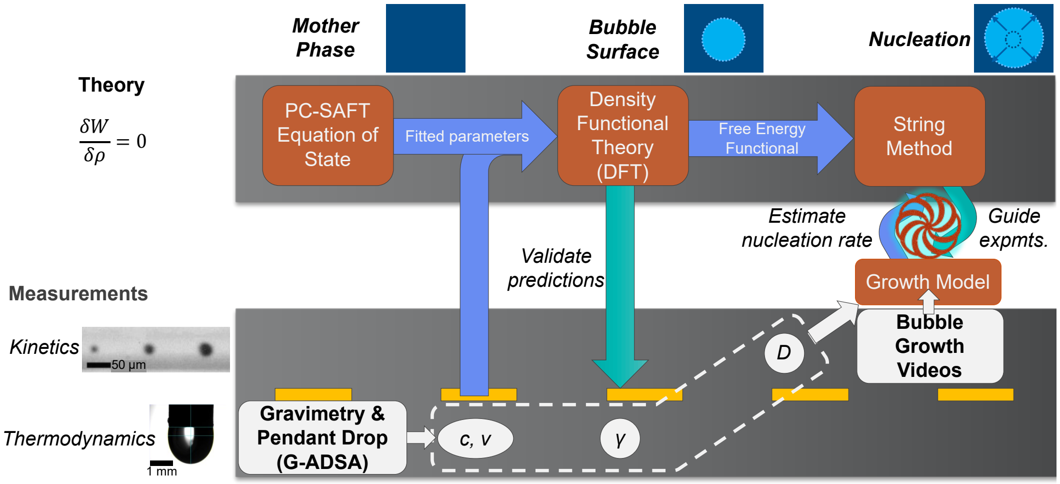

Figure I.13: Roadmap of the cooperation between experiments and theory to understand bubble nucleation. The top track shows the theoretical methods employed, which were largely developed by our collaborator Dr. Huikuan Chao. The bottom two tracks show the experimental methods employed, with kinetic measurements along the top lane and thermodynamic measurements along the bottom lane. The two tracks interact at each level of sophistication of the model: mother phase, bubble surface, and bubble nucleation. The ultimate goal is a synergy between theory and experiment to understand bubble nucleation, with theory guiding experiments toward interesting conditions and experiments testing the predictions of theory, as shown by the Armenian symbol of eternity between the string method and bubble growth model.

## References

1. Jones, S., Evans, G. & Galvin, K. Bubble nucleation from gas cavities a review. *Advances in Colloid and Interface Science* **80,** 27–50. ISSN: 00018686. https://linkinghub.elsevier.com/retrieve/pii/S0001868698000748 (Feb. 1999).
2. Liger-Belair, G. The physics and chemistry behind the bubbling properties of champagne and sparkling wines: A state-of-the-art review. *Journal of Agricultural and Food Chemistry* **53,** 2788–2802. ISSN: 00218561 (2005).
3. Harvey, E. N. *et al.* Bubble formation in animals. I. Physical factors. *Journal of Cellular and Comparative Physiology* **24,** 1–22. ISSN: 0095-9898. https://onlinelibrary.wiley.com/doi/10.1002/jcp.1030240102 (Aug. 1944).
4. Guo, Z. *et al.* CO2 bubble nucleation in polystyrene: Experimental and modeling studies. *Journal of Applied Polymer Science* **125,** 2170–2186. ISSN: 00218995. https://onlinelibrary.wiley.com/doi/10.1002/app.36422 (Aug. 2012).
5. Blander, M. & Katz, J. L. Bubble nucleation in liquids. *AIChE Journal* **21,** 833–848. ISSN: 15475905 (1975).
6. Kraynik, A. M. Foam Flows. *Annual Review of Fluid Mechanics* **20,** 325–357. ISSN: 0066-4189. https://www.annualreviews.org/doi/10.1146/annurev.fl.20.010188.001545 (Jan. 1988).
7. *The Polyurethanes Book* (eds Randall, D. & Lee, S.) ISBN: 0470850418 (Huntsman International LLC, Polyurethanes business, 2002).
8. Zenit, R. & Rodríguez-Rodríguez, J. The fluid mechanics of bubbly drinks. *Physics Today* **71,** 44–50. ISSN: 0031-9228. http://physicstoday.scitation.org/doi/10.1063/PT.3.4069 (Nov. 2018).
9. Collivignarelli, M. C. *et al.* Foams in Wastewater Treatment Plants: From Causes to Control Methods. *Applied Sciences* **10,** 2716. ISSN: 2076-3417. https://www.mdpi.com/2076-3417/10/8/2716 (Apr. 2020).
10. Claudy, P., Létoffé, J. M., Camberlain, Y. & Pascault, J. P. Glass Transition of Polystyrene Versus Molecular Weight. *Polymer Bulletin* **9,** 208–215 (1983).
11. Shafi, M. A., Joshi, K. & Flumerfelt, R. W. Bubble size distributions in freely expanded polymer foams. *Chemical Engineering Science* **52,** 635–644. ISSN: 00092509 (1997).
12. Schiavoni, S., D'Alessandro, F., Bianchi, F. & Asdrubali, F. Insulation materials for the building sector: A review and comparative analysis. *Renewable and Sustainable Energy Reviews* **62,** 988–1011. ISSN: 13640321. https://linkinghub.elsevier.com/retrieve/pii/S1364032116301551 (Sept. 2016).

13. Stirna, U., Beverte, I., Yakushin, V. & Cabulis, U. *Polyurethane and polyisocyanurate foams in external tank cryogenic insulation* 203–244. ISBN: 9783642353352 (2013).

14. Ivashov, S., Razevig, V., Vasiliev, I., Bechtel, T. & Capineri, L. Holographic subsurface radar for diagnostics of cryogenic fuel tank thermal insulation of space vehicles. *NDT and E International* **69,** 48–54. ISSN: 09638695. http://dx.doi.org/10.1016/j.ndteint.2014.10.002 (2015).

15. Burgaz, E. *Polyurethane Insulation Foams for Energy and Sustainability* 1–26. ISBN: 9783030195588 (Springer, Cham, 2019).

16. Szycher, M. *Szycher's handbook of Polyurethanes* 2nd ed., 1–1192. ISBN: 9781439863138 (CRC Press, Boca Raton, FL, 2012).

17. Glicksman, L. R. in *Low Density Cellular Plastics: Physical Basis of Behavior* 104–151 (1994).

18. Booth, L. Radiation Contribution as an Element of Thermal Conductivity. *Journal of Thermal Insulation* **12,** 153–166. ISSN: 0148-8287. http://journals.sagepub.com/doi/10.1177/109719638801200207 (Oct. 1988).

19. Schuetz, M. & Glicksman, L. A Basic Study of Heat Transfer Through Foam Insulation. *Journal of Cellular Plastics* **20,** 114–121. ISSN: 0021-955X. http://journals.sagepub.com/doi/10.1177/0021955X8402000203 (Mar. 1984).

20. Simpson, A., Rattigan, I., Kalavsky, E. & Parr, G. Thermal conductivity and conditioning of grey expanded polystyrene foams. *Cellular Polymers* **39,** 238–262. ISSN: 0262-4893. http://journals.sagepub.com/doi/10.1177/0262489320934263 (Nov. 2020).

21. Notario, B. *et al.* Experimental validation of the Knudsen effect in nanocellular polymeric foams. *Polymer* **56,** 57–67. ISSN: 00323861. https://linkinghub.elsevier.com/retrieve/pii/S0032386114009021 (Jan. 2015).

22. Notario, B., Pinto, J. & Rodríguez-Pérez, M. A. Towards a new generation of polymeric foams: PMMA nanocellular foams with enhanced physical properties. *Polymer* **63,** 116–126. ISSN: 00323861 (2015).

23. Cao, X., James Lee, L., Widya, T. & Macosko, C. Polyurethane/clay nanocomposites foams: processing, structure and properties. *Polymer* **46,** 775–783. ISSN: 0032-3861. https://www.sciencedirect.com/science/article/pii/S0032386104011322 (Jan. 2005).

24. Moreno, J. D. *Radiative transfer and thermal performance levels in foam insulation boardstocks* PhD thesis (Massachusetts Institute of Technology, 1991). https://dspace.mit.edu/handle/1721.1/28004.

25. Tesser, R., Di Serio, M., Sclafani, A. & Santacesaria, E. Modeling of polyurethane foam formation. *Journal of Applied Polymer Science* **92,** 1875–1886. ISSN: 0021-8995. `https://onlinelibrary.wiley.com/doi/pdf/10.1002/app.20170%20https://onlinelibrary.wiley.com/doi/10.1002/app.20170` (May 2004).

26. Golini, P. & Guandalini, M. *Polyurethane Rigid Foams* 2013. `https://patents.google.com/patent/WO2013030101A1/en`.

27. Guo, H. & Kumar, V. Solid-state poly(methyl methacrylate) (PMMA) nanofoams. Part I: Low-temperature CO2 sorption, diffusion, and the depression in PMMA glass transition. *Polymer* **57,** 157–163. ISSN: 00323861. `http://dx.doi.org/10.1016/j.polymer.2014.12.029` (2015).

28. Guo, H., Nicolae, A. & Kumar, V. Solid-state poly(methyl methacrylate) (PMMA) nanofoams. Part II: Low-temperature solid-state process space using CO2 and the resulting morphologies. *Polymer* **70,** 231–241. ISSN: 00323861. `http://dx.doi.org/10.1016/j.polymer.2015.06.031` (2015).

29. Tammaro, D., Astarita, A., Di Maio, E. & Iannace, S. Polystyrene Foaming at High Pressure Drop Rates. *Industrial and Engineering Chemistry Research* **55,** 5696–5701. ISSN: 15205045 (2016).

30. Yang, Z., Hu, D., Liu, T., Xu, Z. & Zhao, L. Strategy for preparation of microcellular rigid polyurethane foams with uniform fine cells and high expansion ratio using supercritical CO2 as blowing agent. *The Journal of Supercritical Fluids* **153,** 104601. ISSN: 1359-0286. `http://dx.doi.org/10.1016/j.cossms.2010.07.001` (2019).

31. Brondi, C. *et al.* Thermosetting polyurethane foams by physical blowing agents: Chasing the synthesis reaction with the pressure. *The Journal of Supercritical Fluids* **154,** 104630. ISSN: 08968446. `https://linkinghub.elsevier.com/retrieve/pii/S0896844619302323` (Dec. 2019).

32. Minogue, E. *An in-situ study of the nucleation process of polyurethane rigid foam formation* PhD thesis (Dublin City University, 2000), 1–194. `http://doras.dcu.ie/19076/`.

33. Reignier, J., Alcouffe, P., Méchin, F. & Fenouillot, F. The morphology of rigid polyurethane foam matrix and its evolution with time during foaming – New insight by cryogenic scanning electron microscopy. *Journal of Colloid and Interface Science* **552,** 153–165. ISSN: 00219797. `https://linkinghub.elsevier.com/retrieve/pii/S0021979719305764` (Sept. 2019).

34. ASTM. *Standard Practice for Polyurethane Raw Materials: Polyurethane Foam Cup Test* 2021. `https://www-astm-org.caltech.idm.oclc.org/d7487-18.html`.

35. Pérez-Tamarit, S., Solórzano, E., Mokso, R. & Rodríguez-Pérez, M. In-situ understanding of pore nucleation and growth in polyurethane foams by using real-time synchrotron X-ray tomography. *Polymer* **166,** 50–54. ISSN: 0032-3861. https://www.sciencedirect.com/science/article/pii/S0032386119300618 (Mar. 2019).

36. Roberts, C. *et al.* Bubblescale observations of polyurethane foam expansion. *AIChE Journal* **68,** e17595. ISSN: 0001-1541. https://onlinelibrary.wiley.com/doi/10.1002/aic.17595 (May 2022).

37. Wong, A., Mark, L. H., Hasan, M. M. & Park, C. B. The synergy of supercritical CO2 and supercritical N2 in foaming of polystyrene for cell nucleation. *Journal of Supercritical Fluids* **90,** 35–43. ISSN: 08968446. http://dx.doi.org/10.1016/j.supflu.2014.03.001 (2014).

38. Leung, S. N. S. *Mechanisms of Cell Nucleation, Growth, and Coarsening in Plastic Foaming: Theory, Simulation, and Experiment* PhD thesis (University of Toronto, 2009), 1–214.

39. Brondi, C., Di Maio, E., Bertucelli, L., Parenti, V. & Mosciatti, T. Competing bubble formation mechanisms in rigid polyurethane foaming. *Polymer* **228,** 123877. ISSN: 00323861. https://doi.org/10.1016/j.polymer.2021.123877%20https://linkinghub.elsevier.com/retrieve/pii/S0032386121005000 (July 2021).

40. Ionescu, M. *Chemistry and Technology of Polyols for Polyurethanes , 2nd Edition Chemistry and Technology of Polyols for Polyurethanes* 2nd ed., 1–548. ISBN: 9781910242988 (iSmithers Rapra Publishing, 2005).

41. Purohit, P., Borgford-Parnell, N., Klimont, Z. & Höglund-Isaksson, L. Achieving Paris climate goals calls for increasing ambition of the Kigali Amendment. *Nature Climate Change.* ISSN: 1758-678X (2022).

42. Akdogan, E., Erdem, M., Ureyen, M. E. & Kaya, M. Rigid polyurethane foams with halogen-free flame retardants: Thermal insulation, mechanical, and flame retardant properties. *Journal of Applied Polymer Science* **137,** 1–14 (2019).

43. Kazarian, S. G. Polymer Processing with Supercritical Fluids. *Polymer Science, Ser. C* **42,** 78–101 (2000).

44. Primel, A. *et al.* Solubility and interfacial tension of thermoplastic polyurethane melt in supercritical carbon dioxide and nitrogen. *Journal of Supercritical Fluids* **122,** 52–57. ISSN: 08968446. http://dx.doi.org/10.1016/j.supflu.2016.11.016 (2017).

45. Tomasko, D. L. *et al.* Development of CO2 for polymer foam applications. *The Journal of Supercritical Fluids* **47,** 493–499. ISSN: 0896-8446. https://www.sciencedirect.com/science/article/pii/S0896844608003586 (Jan. 2009).

46. Arora, K. A., Lesser, A. J. & Mccarthy, T. J. Preparation and Characterization of Microcellular Polystyrene Foams Processed in Supercritical Carbon Dioxide. *Macromolecules* **31,** 4614–4620. https://pubs.acs.org/sharingguidelines (1998).

47. NIST. *NIST Standard Reference Database Number 69* 2022. https://webbook.nist.gov/chemistry/ (2022).

48. Sauceau, M., Fages, J., Common, A., Nikitine, C. & Rodier, E. New challenges in polymer foaming: A review of extrusion processes assisted by supercritical carbon dioxide. *Progress in Polymer Science* **36,** 749–766. ISSN: 00796700. http://dx.doi.org/10.1016/j.progpolymsci.2010.12.004%20https://linkinghub.elsevier.com/retrieve/pii/S0079670010001280%20https://pubs.acs.org/doi/10.1021/la0266381 (June 2011).

49. Jacobs, L. J., Kemmere, M. F. & Keurentjes, J. T. Sustainable polymer foaming using high pressure carbon dioxide: A review on fundamentals, processes and applications. *Green Chemistry* **10,** 731–73. ISSN: 14639270 (2008).

50. Forest, C., Chaumont, P., Cassagnau, P., Swoboda, B. & Sonntag, P. Polymer nano-foams for insulating applications prepared from CO2 foaming. *Progress in Polymer Science* **41,** 122–145. ISSN: 00796700. https://www.sciencedirect.com/science/article/pii/S0079670014000689%20https://linkinghub.elsevier.com/retrieve/pii/S0079670014000689 (Feb. 2015).

51. Miller, D., Chatchaisucha, P. & Kumar, V. Microcellular and nanocellular solid-state polyetherimide (PEI) foams using sub-critical carbon dioxide I. Processing and structure. *Polymer* **50,** 5576–5584. ISSN: 00323861. http://dx.doi.org/10.1016/j.polymer.2009.09.020 (2009).

52. Costeux, S. CO2-blown nanocellular foams. *Journal of Applied Polymer Science* **131,** 41293. http://doi.wiley.com/10.1002/app.41293 (Dec. 2014).

53. Costeux, S. & Zhu, L. Low density thermoplastic nanofoams nucleated by nanoparticles. *Polymer* **54,** 2785–2795. ISSN: 0032-3861. https://www.sciencedirect.com/science/article/pii/S0032386113002711 (May 2013).

54. Zhao, J., Wang, G., Zhang, A., Zhao, G. & Park, C. B. Nanocellular TPU composite foams achieved by stretch-assisted microcellular foaming with low-pressure gaseous CO2 as blowing agent. *Journal of CO2 Utilization* **53,** 101708 (Nov. 2021).

55. Yokoyama, H. & Sugiyama, K. Nanocellular structures in block copolymers with CO2-philic blocks using CO2 as a blowing agent: Crossover from micro- to nanocellular structures with depressurization temperature. *Macromolecules*

**38,** 10516–10522. ISSN: 00249297. https://pubs.acs.org/doi/10.1021/ma051757j (Dec. 2005).

56. Debenedetti, P. G. *Metastable Liquids* 147–176. ISBN: 0-691-08595-1 (Princeton University Press, Princeton, NJ, 1996).
57. Diemand, J., Angélil, R., Tanaka, K. K. & Tanaka, H. Large scale molecular dynamics simulations of homogeneous nucleation. *The Journal of Chemical Physics* **139,** 074309. ISSN: 0021-9606. arXiv: 1308.0972. http://aip.scitation.org/doi/10.1063/1.4818639 (Aug. 2013).
58. Volmer, M. & Weber, Keimbildung in übersättigten Gebilden. *Zeitschrift für Physikalische Chemie* **119U,** 277–301. ISSN: 2196-7156. https://www.degruyter.com/document/doi/10.1515/zpch-1926-11927/html (Jan. 1926).
59. Gibbs, J. W. *The Scientific Papers of JW Gibbs* (Dover, 1961).
60. Farkas, L. Nucleation Rates in Supersaturated Vapours. *Z. Phys. Chem.* **125,** 236 (1927).
61. Kaischew, R. & Stranski, I. N. Zur kinetischen Ableitung der Keimbildungsgeschwindigkeit. *Zeitschrift für Physikalische Chemie* **26B,** 317–326. ISSN: 2196-7156. https://www.degruyter.com/document/doi/10.1515/zpch-1934-2628/html (June 1934).
62. Becker, R. & Döring, W. Kinetische Behandlung der Keimbildung in übersättigten Dämpfen. *Annalen der Physik* **416,** 719–752. ISSN: 00033804. https://onlinelibrary.wiley.com/doi/10.1002/andp.19354160806 (1935).
63. Zeldovich, J. Theory of Nucleation and Condensation. *Sov. Phys. JETP* **12,** 525 (1942).
64. Kagan, Y. The Kinetics of Boiling of a Pure Liquid. *Russ. J. Phys. Chem.* **34** (1960).
65. Talanquer, V. & Oxtoby, D. W. Nucleation of bubbles in binary fluids. *The Journal of Chemical Physics* **102,** 2156–2164. ISSN: 0021-9606. http://aip.scitation.org/toc/jcp/102/5%20http://aip.scitation.org/doi/10.1063/1.468737 (Feb. 1995).
66. Kalikmanov, V. I. in *Lecture Notes in Physics* 1–331 (2013). ISBN: 9789048136421.
67. Oxtoby, D. W. Homogeneous nucleation: theory and experiment. *Journal of Physics: Condensed Matter* **4,** 7627–7650. ISSN: 0953-8984. https://iopscience.iop.org/article/10.1088/0953-8984/4/38/001 (Sept. 1992).
68. Skripov, V. P. *Metastable Liquids* 1–264. ISBN: 0-470-79546-8 (Halsted Press, New York, NY, 1974).

69. Ando, K., Liu, A. Q. & Ohl, C. D. Homogeneous nucleation in water in microfluidic channels. *Physical Review Letters* **109,** 044501. ISSN: 00319007 (2012).

70. Goel, S. K. & Beckman, E. J. Generation of microcellular polymeric foams using supercritical. *Polymer Engineering and Science* **34,** 1137–1147 (1994).

71. Wang, R. & Wang, Z. G. Theory of polymers in poor solvent: Phase equilibrium and nucleation behavior. *Macromolecules* **45,** 6266–6271. ISSN: 00249297 (2012).

72. Flagan, R. C. A thermodynamically consistent kinetic framework for binary nucleation. *Journal of Chemical Physics* **127,** 1–7. ISSN: 00219606 (2007).

73. Xu, X., Cristancho, D. E., Costeux, S. & Wang, Z.-G. Bubble nucleation in polymer–CO2 mixtures. *Soft Matter* **9,** 9675. ISSN: 1744-683X. `www.rsc.org/softmatter%20http://xlink.rsc.org/?DOI=c3sm51477c` (2013).

74. Sleutel, M., Lutsko, J., Van Driessche, A. E., Durán-Olivencia, M. A. & Maes, D. Observing classical nucleation theory at work by monitoring phase transitions with molecular precision. *Nature Communications* **5.** ISSN: 20411723 (2014).

75. Kim, Y., Park, C. B., Chen, P. & Thompson, R. B. Origins of the failure of classical nucleation theory for nanocellular polymer foams. *Soft Matter* **7,** 7351–7358. ISSN: 1744683X (Aug. 2011).

76. Costeux, S., Khan, I., Bunker, S. P. & Jeon, H. K. Experimental study and modeling of nanofoams formation from single phase acrylic copolymers. *Journal of Cellular Plastics* **51,** 197–221 (2015).

77. Cahn, J. W. & Hilliard, J. E. Free Energy of a Nonuniform System. III. Nucleation in a TwoComponent Incompressible Fluid. *The Journal of Chemical Physics* **31,** 688–699. ISSN: 0021-9606. `http://aip.scitation.org/doi/10.1063/1.1730447` (Sept. 1959).

78. Müller, M., MacDowell, L. G., Virnau, P. & Binder, K. Interface properties and bubble nucleation in compressible mixtures containing polymers. *The Journal of Chemical Physics* **117,** 5480–5496. ISSN: 0021-9606. `http://aip.scitation.org/doi/10.1063/1.1497636` (Sept. 2002).

79. Xu, X., Cristancho, D. E., Costeux, S. & Wang, Z.-G. Discontinuous Bubble Nucleation Due to a Metastable Condensation Transition in Polymer–CO2 Mixtures. *The Journal of Physical Chemistry Letters* **4,** 1639–1643. `http://pubs.acs.org/doi/10.1021/jz4005575` (May 2013).

80. E, W., Ren, W. & Vanden-Eijnden, E. String method for the study of rare events. *Physical Review B* **66,** 052301. ISSN: 0163-1829. `https://link.aps.org/doi/10.1103/PhysRevB.66.052301` (Aug. 2002).

81. E, W., Ren, W. & Vanden-Eijnden, E. Simplified and improved string method for computing the minimum energy paths in barrier-crossing events. *The Journal of Chemical Physics* **126,** 164103. ISSN: 0021-9606. http://jcp.aip.org/jcp/copyright.jsp%20http://aip.scitation.org/doi/10.1063/1.2720838 (Apr. 2007).

82. Zhang, C. Z. & Wang, Z. G. Nucleation of membrane adhesions. *Physical Review E* **77,** 021906. ISSN: 15393755 (2008).

83. Di Maio, E. & Kiran, E. Foaming of polymers with supercritical fluids and perspectives on the current knowledge gaps and challenges. *The Journal of Supercritical Fluids* **134,** 157–166. ISSN: 08968446. https://www.sciencedirect.com/science/article/pii/S0896844617307593 (Apr. 2018).